Timing, volume and precursory indicators of rock- and cliff fall on a permafrost mountain ridge (Mattertal, Switzerland)

Hanne Hendrickx, Gaëlle Le Roy, Agnès Helmstetter, Eric Pointner, Eric Larose, Luc Braillard, Jan Nyssen, Reynald Delaloye, Amaury Frankl

Integration of high resolution records for understanding the processes behind a disintegrating permafrost rock face, Mattertal, Switzerland.

Abstract: Rockfall sites often represent a challenging study object due to a complex interaction between site-specific conditions such as geology, topography and meteorology on the one hand and their inaccessibility on the other hand. Therefore, the combination of several close-range remote sensing techniques were used to offer a detailed account of 339 rock- and cliff fall events (< 10 – 31 300 m^3) observed in a timespan of four years (2017-2020) at a south facing rock face at Grosse Grabe in Mattertal (Western Swiss Alps), depositing more than 200 000 m^3 of debris. Large cliff falls (10^4-10^6 m^3) were preluded by an outward movement that started to increase 1.5 years before any significant collapse of the rock face and reaching locally up to 30 cm. This progressive displacement of the rock face was more pronounced in summer, indicating thermal induced failure mechanism were at play at fracture level. In addition, ice cementation in the clefts could have played a stabilising role in the winter. The largest cliff fall events occurred in summer and systematically exposed ice in the clefts. This is assumed to be the base of the permafrost from the north side, because the collapsing south face is unsuitable for permafrost to occur. The presented dataset is unique because data collection started before the onset of the rock wall destabilisation and collapse, allowing to get insight into the processes at play prior to large rock- and cliff fall. Highly fractured south-exposed gneiss lithology is viewed as the main precondition for the observed rockfall events, allowing high temperature oscillations to cause irreversible movements at fracture level. Rapid permafrost degradation is viewed as a triggering factor after its exposure, causing progressive failure of the rock wall leading to very high rock wall erosion rates on a decadal timescale.

Keywords: Terrestrial laser scanner, photogrammetry, rockfall, seismology, mountain permafrost, structural predisposition

---

1. Introduction

Rockfall, i.e. the downward free or bounding movement of rock detachments from steep rock walls, is a common geomorphic phenomenon in steep relief (Luckman, 2013) and an important rockwall erosion agent (Krautblatter and Moore, 2014). Rockfall usually describes detachments of a magnitude up to 10^4 m^3 (Dussauge, Grasso and Helmstetter, 2003), ranging from boulder falls (10^1-10^2 m^3), debris falls (< 10^3 m^3) and block falls (10^2-10^4 m^3) (Krautblatter, Funk and Günzel, 2013). Larger magnitude events are defined as cliff falls (10^4-10^6 m^3), rockslides and rock avalanches (>10^6 m^3) (Krautblatter, Funk and Günzel, 2013). Geological structures and related fracture geometry and density are important predisposition factors for rock wall instability leading to rockfall (Gunzburger, Merrien-Soukatchoff and Guglielmi, 2005; Hasler, Gruber and Beutel, 2012; Beniston *et al.*, 2018). Temperature oscillations, both on daily, seasonal and annual timescales, can serve as a potential preparatory factor. The expansion and contraction of rock can cause thermal stress fatigue and small irreversible displacements of rock fractures (Gunzburger, Merrien-Soukatchoff and Guglielmi, 2005; Collins and Stock, 2016; Weber *et al.*, 2017; Bakun-Mazor *et al.*, 2020). When seasonal or permanent ice is present in the rock wall, temperature cycles drive cryogenic processes such as ice segregation and volumetric expansion (Matsuoka, 2008), leading to rockwall erosion by frost weathering (Krautblatter and Dikau, 2007; Draebing and Krautblatter, 2019). Rockfall is therefore particularly common in the high mountain environment experiencing seasonal frost or permafrost (Fischer *et al.*, 2012; Ravanel, Magnin and Deline, 2017). In periglacial areas, rockfall events mostly occur in the warm half of the year (Sass, 2005c), triggered for example by rainfall (Helmstetter and Garambois, 2010; Dietze, Turowski, *et al.*, 2017), diurnal temperature changes (Dietze, Turowski, *et al.*, 2017) and freeze-thaw transitions (Luckman, 2013; Dietze, Turowski, *et al.*, 2017). Because of this, rockfall activity is often higher during spring and autumn (Gardner, 1983; Luckman, 2013; Dietze, Turowski, *et al.*, 2017). North-facing rockwalls also experience more frost action due their high moisture levels and lower average temperatures, leading to enhanced rockfall activity (Gardner, 1983; Sass, 2005b). This highlights that climatic factors are crucial for rock wall stability as well, since they control weathering processes (Sass, 2005a; Draebing and Krautblatter, 2019) and affect bedrock permafrost, the latter possibly subjected to fast change (Gruber and Haeberli, 2007). In this context, climate change can modify the rockfall susceptibility and the related hazard risk (Haeberli and Beniston, 1998). Warming permafrost and increasing seasonal thaw depth can alter the stability of steep rock faces (Noetzli *et al.*, 2007; Fischer *et al.*, 2012; Draebing, Krautblatter and Dikau, 2014) by the failure of ice-filled rock fractures due the lowering of shear resistance with increasing temperature (Davies, Hamza and Harris, 2001). Areas characterized by warm permafrost (between -2°C and 0°C) will first be affected by this process. For mountains flanked by densely populated areas, like the European Alps, rockfall is particularly hazardous, affecting communities, infrastructures and economies at lower elevations (Gruber and Haeberli, 2007; Walter *et al.*, 2019).

In the last three decades, an increase rockfall events (< 10^4 m^3) have been observed in permafrost areas in many places of the European Alps, often related to summer heatwaves that cause excessive permafrost thawing from the surface, deepening the active layer (Gruber, 2004; Fischer *et al.*, 2011; Stoffel and Huggel, 2012; Ravanel, Magnin and Deline, 2017). An increase in larger rockfall or cliff fall events (10^4-10^6 m^3) has been observed as well (Fischer *et al.*, 2012), caused by failure at greater depth as the consequence of a gradual permafrost degradation, rather than active layer thaw (Gruber and Haeberli, 2007; Allen and Huggel, 2013). Very large rock slope failures, often referred to as rockslides or rock avalanches (> 10^6 m^3), can occur at any time of the year (Phillips *et al.*, 2017) and are not necessarily linked to areas where warm permafrost occurs (Hasler *et al.*, 2011). In these cases, the rockfall occurrence is primarily controlled by the lithological settings of the site (Fischer *et al.*, 2012) and by the slow change in fracture toughness of rock bridges due to warming (Krautblatter, Funk and Günzel, 2013). Unprecedented large scale cliff falls, rockslides and rock avalanches may substantially affect the alpine sediment cascade, providing fragmented rock debris on talus slopes, glaciers, rock glaciers and in high alpine torrents. Such unconsolidated sediments may for instance be remobilized by rainfall-triggered debris flows and cause infrastructural damage to downstream communities long after the initial rockfall event (Baer *et al.*, 2017).

To increase the understanding of rock wall instability and its development, important for predicting process dynamics and mitigating hazards (McColl and Draebing, 2019), related rockfall frequencies and magnitudes need to be monitored (Fischer *et al.*, 2012). Terrestrial laser scanning (TLS) and Uncrewed Aerial Vehicle (UAV) data can provide accurate 3D-information about rock face geometry, allowing to derive rockfall location and volume when repeated measurements are done. Precursory indicators before failure such as cleft opening or pre-failure deformation of a few cm can also be detected if the accuracy of the method allows it (Abellán *et al.*, 2010). However, multiple rockfall releases within one monitoring period cannot be resolved using TLS/UAV data (Dietze, Mohadjer, *et al.*, 2017). Automatic camera images can help identify different events, but only when visibility allows it (and thus e.g. not during the night or foggy conditions). Rockfall events can also be studied by analysing the characteristic seismic pulses they cause. In contrast to TLS/UAV data, seismic data does not rely on survey intervals (Dietze, Mohadjer, *et al.*, 2017; Le Roy *et al.*, 2019) or visibility conditions (Dietze, Mohadjer, *et al.*, 2017). Seismic data can therefore be used for real-time detection and warning. Moreover, the link between external factors influencing the rockfall event can be studied better if the exact timing of the latter is known (Dietze, Mohadjer, *et al.*, 2017; Le Roy *et al.*, 2019). Relationships between rockfall event properties (detachment and impact areas, volume, geometry and propagation) and the seismic signal can also be applied in different geological settings and for different rockfall magnitudes (Le Roy *et al.*, 2019). Combining different datasets is therefore essential for rockfall characterisation (Fischer *et al.*, 2011; Dietze, Mohadjer, *et al.*, 2017). Although it is rare to have data from initial destabilisation up to failure of a rock face, this information is of high importance for adopting early warning systems (Leinauer, Jacobs and Krautblatter, 2020).

The main aim of this study is to accurately present the temporal and spatial distribution of all rockfall events that occurred at a disintegrating south-facing rock face (2600 – 2700 m a.s.l.) in Mattertal, Switzerland. To achieve this, a combination and integration of four different datasets (UAV, TLS, seismic and automatic camera data) were used. By doing so, this study provides valuable information for rockfall hazard management and contributes toward the understanding of the processes involved in large rock- and cliff fall, having increasingly occurred in high mountain environments during the last three decades (Huggel *et al.*, 2012). While post-event remote sensing is common to study rockfall in the periglacial high mountain environment (Fischer *et al.*, 2011; Dietze, Mohadjer, *et al.*, 2017; Le Roy *et al.*, 2019; Sala, Hutchinson and Harrap, 2019), it is rare to have direct observations before, during, and after rockfall. Here, we present such a unique dataset (2017 – 2020), resulting in valuable information about precursory processes, temporal distribution and potential triggers of rockfall. This study benefited greatly from the datasets available from seismic and automatic camera installations, already in place for rock glacier monitoring and their relationship to debris flow activity (Kummert, Delaloye and Braillard, 2018; Guillemot *et al.*, 2020).

2. Study site, material and methods

Table 1.: Overview of application and integration of the various methods used in this study

			Fixed installations for the monitoring of rock glaciers	
	TLS	UAV	Seismics	Time-lapse camera
Start of the monitoring	2017	2020	2015	2011
Temporal resolution	Bi-annual (10 scans)	Weekly (5 surveys)	Continuous	Hourly
Spatial accuracy	3 cm	30 cm	Low, only one logger	High qualitative confirmation of rockfall
Spatial extent	Grosse Grabe North Pillar and adjacent rock wall	Grosse Grabe North Pillar	Grosse Grabe North Pillar, South pillar and environments	Grosse Grabe North Pillar
Remarks	• Topographic occlusion due to single scan position • Cumulative volumes • Precursory deformation	• No topographic occlusion • Visual information • Event based volumes	• All rockfall recorded • Estimated volumes • No exact rockfall location	• Near real-time confirmation of rockfall and location • Precursory fracture widening • Qualitative data

TLS: terrestrial laser scanning, UAV: uncrewed aerial vehicle

2.1. Study area

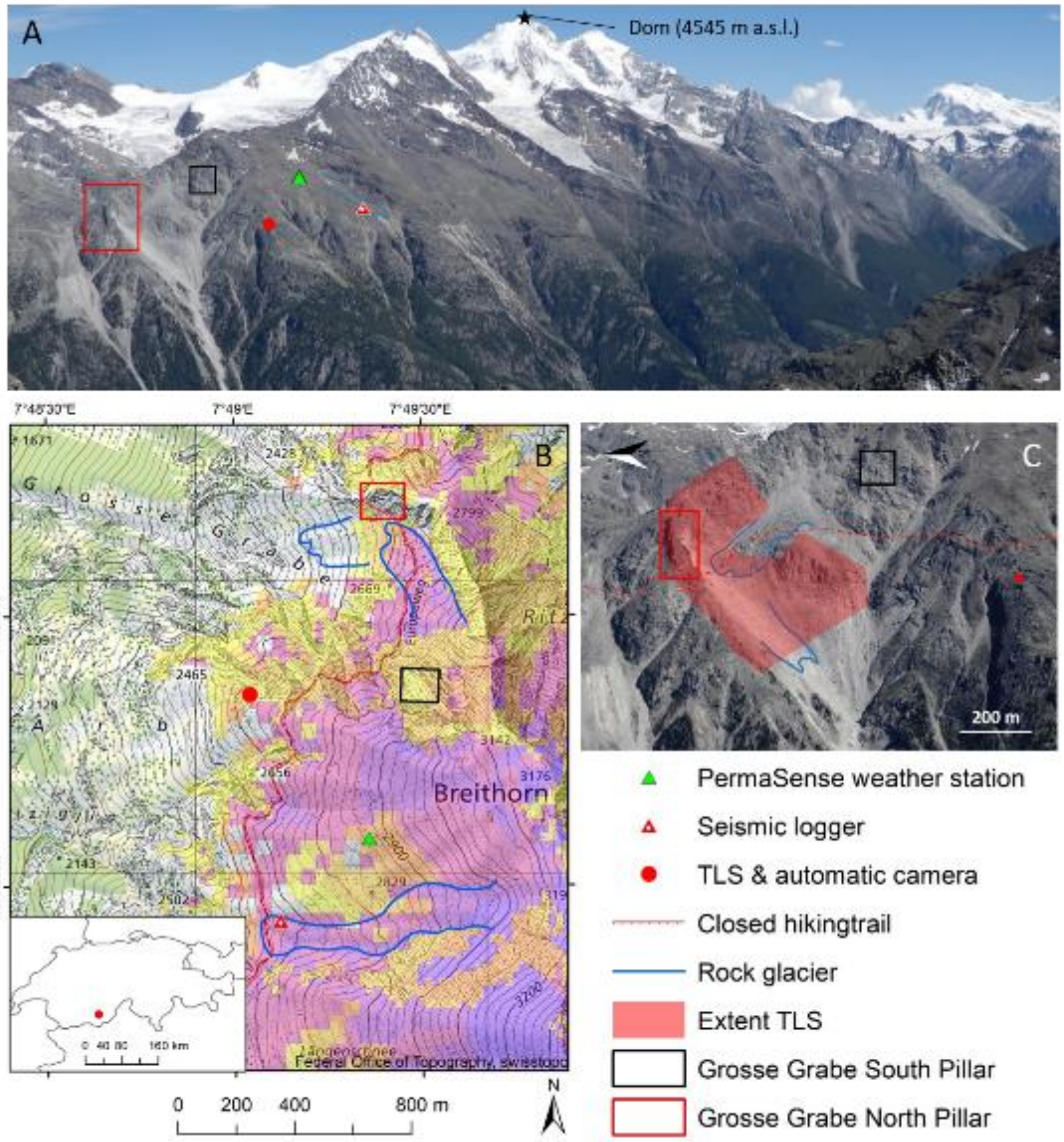

Figure 1.: The study area: a) The environment of the rock face studied and the monitoring installations in place for the study of nearby rock glaciers, together with the position of the laserscan, which was specifically executed for the monitoring of Grosse Grabe North Pillar. The Dom is the highest summit of the area at 4545 m a.s.l. and the treeline is located at about 2300 m a.s.l., b) Potential permafrost distribution in the environment displayed on the topographic map (SwissTopo), ranging from yellow for patchy permafrost in favourable conditions and dark purple/blue for extensive permafrost in nearly all conditions (Boeckli *et al.*, 2012), c) insert of the study area, displaying the extent of the terrestrial laser scans.

The study area is an unstable south-facing rock face (2600 – 2700 m a.s.l.), North of the Grosse Grabe torrent (and hereafter referred to as Grosse Grabe North Pillar) and its adjacent rock wall, at the orographic right side of the Mattertal valley, Switzerland (46°09'08"N, 7°49'21"E, Figure 1). The lithological structure consists of highly fractured augen gneiss with a foliation dipping

SW, interlaced with various tectonic cleft structures (Bearth, 1978). The studied rock face is part of a narrow ridge with a height of 100 – 120 m. The first monitored rock fall activity at Grosse Grabe North Pillar occurred in the mid-1980s, as observed in historical aerial photographs (Figure 2b, Delaloye *et al.*, 2014). The rock glacier at the base of the rock face was overburdened by these deposits and reaccelerated rapidly (velocities up to 5 m per year between 1995 and 2010). Because of this, the upper and currently intact part of the rock glacier, not impacted by the rockfall of the 1980s, is separated from the lower terminal tongue (Figure 2c-d, Delaloye *et al.*, 2013). The movement of the terminal tongue has been decreasing since 2010 (Delaloye *et al.*, 2013) and had become very slow when the survey of the lower section stopped in 2017 (< 0.5 m/yr). This marks the end of the destabilisation phase of the rock glacier, likely indicating the almost completed permafrost degradation at depth, in analogy to the attested absence of permafrost in the well-developed rupture zone of a similarly destabilised rock glacier (Delaloye and Morard, 2011). Rock wall instabilities in the surroundings of the study area are common as well, with isolated rockfall from the same ridge in the 1970s (Figure 2a, Delaloye *et al.*, 2014). More recent rockfall from an area more to the south of the studied rock face (Grosse Grabe South Pillar, Figure 1) led to the closure of the hiking trail crossing the area in 2018.

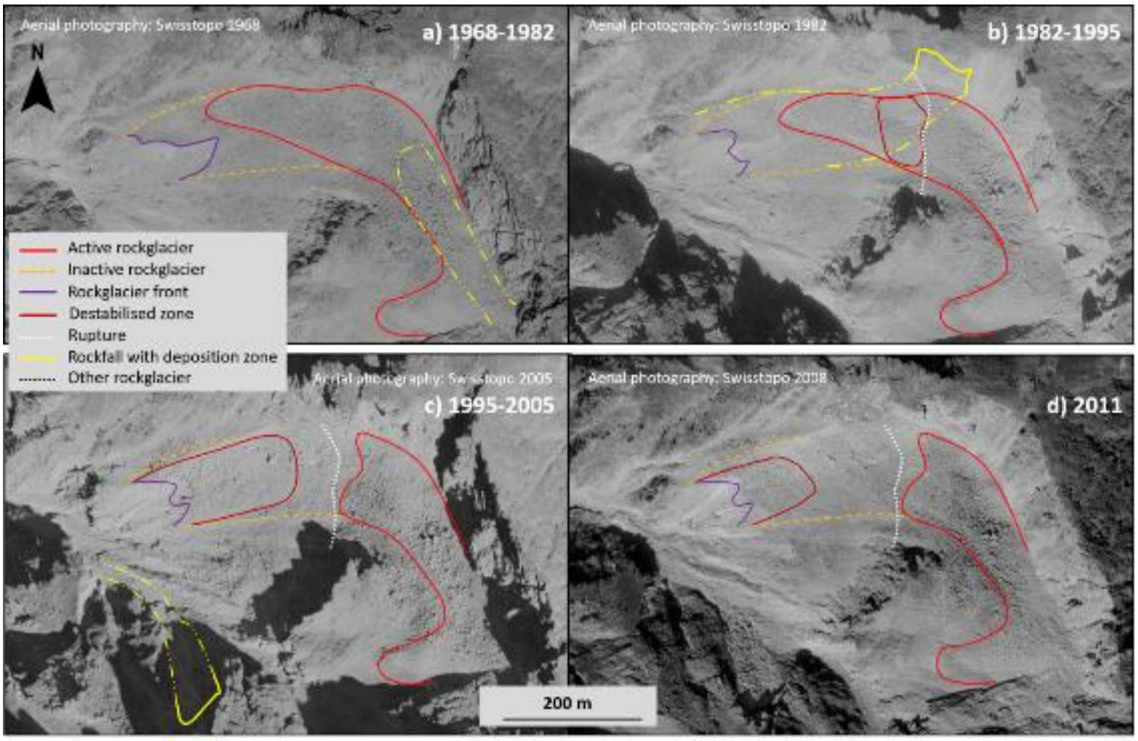

Figure 2. Orthophotos revealing the historical development of the site related to rockfall activity, a) isolated rockfall from the same ridge occurring in the 1970s, b) rockfall from Grosse Grabe North Pillar occurring in the mid-1980s, overburdening the rock glacier below, c) and d) the development of the rupture of the rock glacier.

The studied rock face is below the lower limit of permafrost occurrence of south faces, which is around 3300 m a.s.l. in the Mont Blanc Massif (Magnin *et al.*, 2017) and around 2900 m a.s.l. in the Swiss Alps, for ice-poor permafrost (Kenner, Noetzli, *et al.*, 2019). However, permafrost may exist in the studied rock wall because of the opposite north face, here in a distance of approx. 50 – 70 m across the pillar. Indeed, the potential permafrost distribution map shows that local permafrost likely to be found at the north face and absent at the south face of Grosse Grabe (Figure 1, Boeckli *et al.*, 2012). Moreover, the highly fractured bedrock favours bedrock cooling by the convection of cold air (Moore *et al.*, 2011) and the trapping of snow in winter time (Hasler, Gruber and Haeberli, 2011). All of the above makes permafrost presence in the studied rock wall likely.

2.2. Meteorological data

A long term record of high temporal resolution meteorological data is available from Grächen station (MeteoSwiss, 46°11’42”N, 7°50’09”E at 1605 m a.s.l., approx. 5 km from the study area, same orographic side of the valley); this meteorological station has measured air temperature and precipitation since 1864, with automatically measured data available since 2013. Annual mean precipitation at this station is 625 ± 120 mm for the reference period of 1981 – 2010. There is low seasonality in precipitation, with October the wettest month (63 ± 52 mm), and January through April the driest months (30–40 mm on average) (Stoffel, Tiranti and Huggel, 2014, MeteoSwiss). Mean annual air temperature (MAAT) at the meteorological station is around 5.3 ± 0.7 °C (1981-2000) (MeteoSwiss). A shorter temperature record (2012-2020) with a 2-minute interval is available from a weather station located on the Breithorn landslide (2873 m a.s.l.), 1 km from the study area (Figure 1), revealing a MAAT of -0.3 ± 0.7 °C. This weather station is deployed by PermaSense, a consortium of researchers and research projects developing and operating autonomous sensing systems in high-mountain environments for acquiring long-term datasets (*UZH - The PermaSense Consortium*, 2021). Temperature data of the PermaSense station correlates well linearly with the temperature record of Grächen (R^2 = 0.97), corresponding to a lapse rate of 4.9 ± 1.03 C° km^{-1}. This linear relationship justifies the use of the Grächen temperature record when data gaps occur in the PermaSense station. Within this study, temperature and precipitation data is used to detect relationships between rockfall and frost/thaw and wet/dry cycles, as shown by other studies (Helmstetter and Garambois, 2010; Bajni, Camera and Apuani, 2020). To do this, the cross-correlation function was established between temperature or precipitation data from the more complete Grächen series and the rate of rockfalls detected from the seismic network. This highlights the potential triggering effect of precipitation/temperature without defining a threshold and provides the time delay between a certain meteorological event and the occurring rockfall. For a detailed description of the methodology, see Helmstetter and Garambois (2010). Local temperature data from the PermaSense station was used to detect if any specific event preluded the largest rock – and cliff fall observed (> 5000 m^3), using a simple t-test comparing weekly temperature averages on the 95% significance level.

2.3. Hourly terrestrial time-lapse photography

Monitoring of rockfall occurrence can be achieved by photographic surveys using fixed installations (D'Amato *et al.*, 2016; Matsuoka, 2019). In this study, the observation of the rock face started in 2011 with the hourly archival of images taken by an automatic camera (Table 1, Figure 3). The latter was installed to study the rock glaciers underneath the face and its connection to the torrent prone to debris flows (Delaloye *et al.*, 2013; Kummert, Delaloye and Braillard, 2018). This offers a near real-time visual check of the Grosse Grabe North pillar, detecting the first rockfall events in the winter of 2017 and dating and locating the rockfall events thereafter, similar to D'Amato *et al.* (2016). The automatic camera imagery also revealed that some parts of the pillar showed precursory deformation before 2017 (Figure S1, Suppl. Material), but as the motion was mostly directed towards the camera, it was not possible to quantify it reliably. The automatic camera is powered by an 80 W solar panel which charges a 12 V battery. This battery is also used to power a router which transfers the hourly images to a server. Near real-time images and selected time lapse sequences can be accessed via the webpage of the Geomorphology research group of Fribourg University (*Study sites - Grosse Grabe*, 2021).

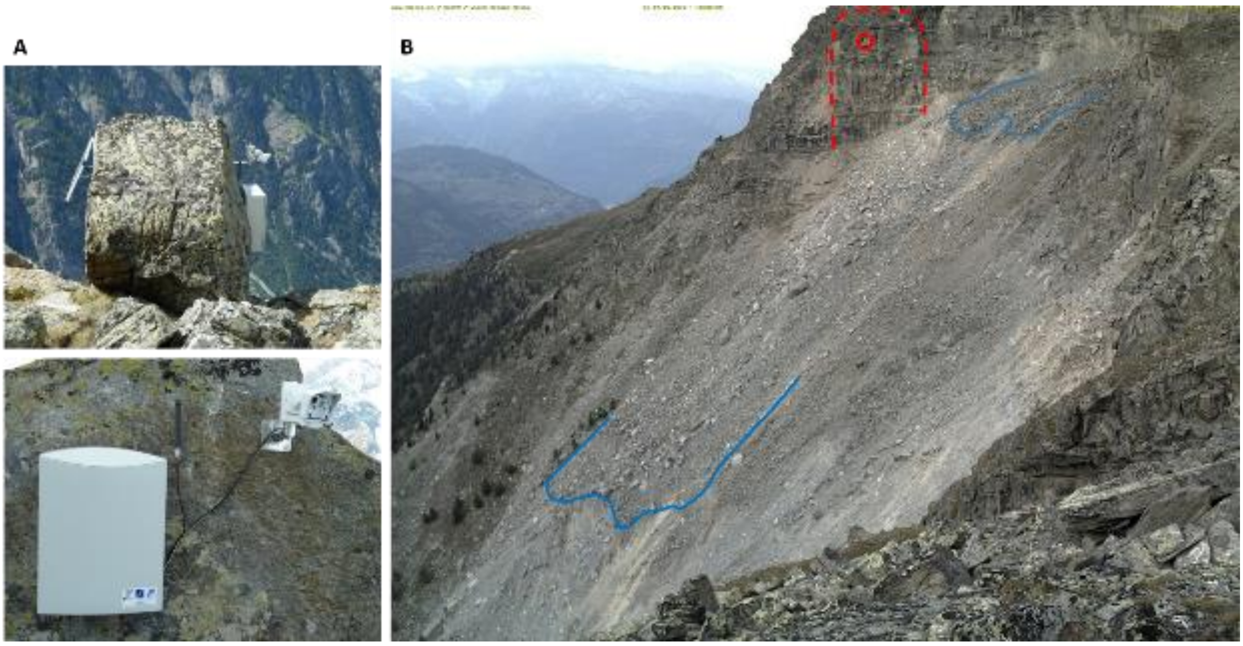

Figure 3.: Set-up of the hourly terrestrial time-lapse photography: a) the installed automatic camera on a large boulder on stable bedrock and b) example of a photograph taken by the automatic camera, displaying the situation before the summer of 2019, indicating the unstable Grosse Grabe North Pillar (striped line), the location of the small scale 2017 rockfall (red circle) and the rock glaciers (blue lines) as the initial subject of study.

2.4. Detailed topographic data derived from terrestrial laser scans and Uncrewed Aerial Vehicle photographs

Terrestrial laser scans (TLS) of the study area were performed from 2017 to 2020 at the beginning (late June/early July) and end (late September/early October) of the summer season (Table 1), using an ultra-long-range near-infrared pulse-based Riegl VZ®-6000 LiDAR system. This LiDAR system allows for a rapid survey (up to 222 000 measurements per second) and permits scans at a large distance from the area of interest (in this case ca. 700 m) (Figure 1). The TLS scan provides high-resolution 3-dimensional point cloud data from the upper talus slope, the upper rock glacier front, Grosse Grabe North Pillar and the adjacent rockwall (Figure 1 c). Starting in 2020, additional scans were executed at the same place to get topographic data from the lower part of the talus slope/rock glacier below to investigate the rockfall deposits. The resulting point clouds were post-processed in RiScanPro® software (version 3.3.438). Data were registered relatively to each other in a local coordinate system using the first scan of geomorphologically stable areas as a reference such as developed by Fischer *et al.* (2016) and Kummert and Delaloye (2018). The multi-station adjustment of all scans achieved an accuracy of 0.03 m as the overall standard deviation of the normal distances and is used as the Level of Detection (LoD). The residuals of the corresponding stable areas between the reference scan and the registered scan showed Gaussian distributions. The resulting point cloud was subsampled to a minimum point spacing of 0.10 m using RiScanPro®'s octree filter.

Uncrewed Aerial Vehicle (UAV) photographs were gathered after large rock- and cliff fall events in the summer of 2020 (Table 1) to improve the frequency of observations and to obtain observations in areas not detectable from the TLS survey position due to topographic occlusion. The UAV imagery was also used to make post-failure observations, allowing to visually detect if massive ice is present in the rockfall scar. Five flights were performed with a DJI Phantom 4 Pro and flown without specific flight planning. Given the inaccessibility of the site no ground control points were placed or measured. The same software and workflow as in Hendrickx *et al.* (2020) were used for processing the photographs into point clouds (See Suppl. Material for more details). To obtain data with high comparative accuracy, the co-alignment methodology was adapted, based on the automatic detection of common tiepoints in the stable areas. A small percentage of these common tiepoints (0.4 - 1%) is sufficient to enforce a common geometry (Cook and Dietze, 2019). For Grosse Grabe, the five UAV surveys share 9% of the total tiepoints. This resulted in a point cloud time-series with 0.30 m as the LoD, calculated on the average change measured in the stable areas (Cook and Dietze, 2019), compared to 1-2 m of detected change in the stable areas when the co-alignment method was not adopted. The resulting UAV derived 3D-models were used for the mapping and the measurements of the geological structures, using the ShapeMetric3D software v3.7.1 (*ShapeMetric3D*, 2021).

Point clouds derived from TLS and UAV data were further analysed in CloudCompare (version 2.11). The Multiscale Model to Model Cloud Comparison (M3C2, normal and projection = 0.6 m, calculated on all the points, minLoD as registration error, preferred orientation in –Y), developed by Lague, Brodu and Leroux (2013), was used to quantify a 3D change accurately to detect deformation of the rock face prior to any rockfall. The function "compute cloud/cloud distance" was used to quickly identify rockfall zones. Both individual and cumulative rockfall volumes were calculated by fitting a plane through the affected rock face and applying the resulting matrix values on the entire point cloud using the 'Apply transformation tool'. This way, 2.5D volumes were calculated in the Z direction, taking the LoD into account. When consecutive rockfall did not affect the same zone, rockfall volumes from individual events could be derived from TLS/UAV data. Therefore, individual TLS volumes are only available for the first rockfall events in the winter and spring of 2017 and 2018. Otherwise, cumulative rockfall volumes spanning the monitoring interval were used to establish a relationship between the measured seismic parameters. The total rockfall volume derived from the TLS data was used to calculate rock wall erosion rate for the entire period of direct observation (2011-2021), including observations from the automatic camera that confirmed no significant rockfall events between 2011 and 2017. The resulting mean annual rockfall volume (m^3) was divided by the slope-perpendicular surface area (m^2) of the studied rockwall (Figure 1 c, TLS extent), similar to the methods used in Hartmeyer *et al.*, (2020).

2.5. Seismic observations

To obtain the exact timing of the rockfall events, we used seismic data of one seismometer (Table 1), part of a network of six seismometers that have been installed to monitor Gugla rock glacier (Guillemot et al., 2020), located 2 km away from the rock face (Figure 1). This sensor was the only one providing continuous data during this study (2017-2020). The sensor is a Sercel L22 one-component geophone with a resonance frequency of 2 Hz (flat response above this frequency) and the signal is recorded continuously at a sampling rate of 200 Hz since 2015. No significant rockfall was detected from the study site before 2017.

We analysed all seismic events within the time interval of events detected by the automatic camera. We selected all events with a peak ground velocity larger than 10 µm s^{-1} and characteristics typical of rockfall seismic signals (Helmstetter and Garambois, 2010; Le Roy *et al.*, 2019): a duration longer than 20 s and an energy content in the range 1-20 Hz. The seismic signal of the largest event is shown in Figure 4. We also checked visually all signals to manually remove earthquake pulses, which show a typical separate arrival of P- and S-wave and long-lasting decreasing tail (coda) (Dietze, Turowski, *et al.*, 2017).

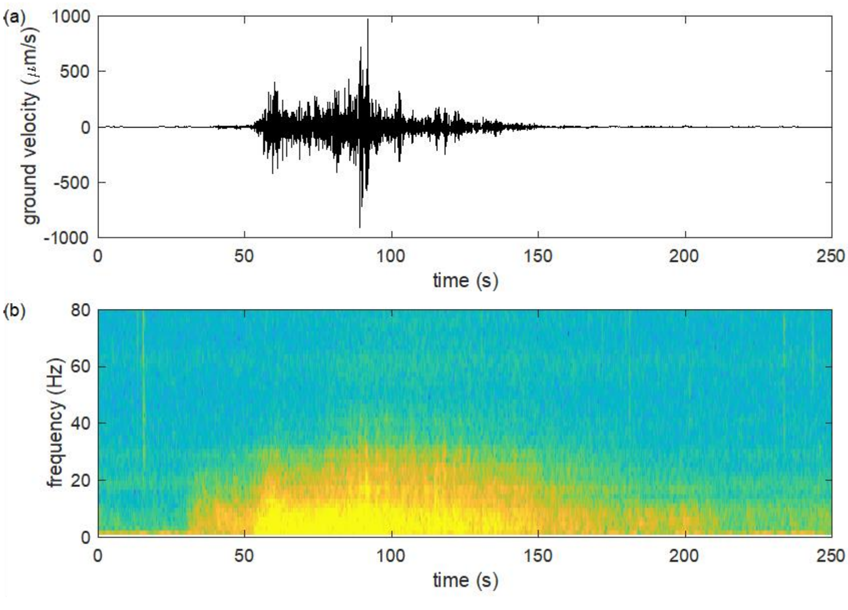

Figure 4. Seismogram (a) and spectrogram (b) for the largest event that occurred on 14 August 2020 at 10:59 UTC time.

We then estimated the seismic energy of each event assuming a point-source (Kanamori and Given, 1982; Eissler and Kanamori, 1987) because the source-sensor distance is much larger than the source area, considering the medium as isotropic and homogeneous. We also considered that surface waves dominate the seismic signal (Deparis *et al.*, 2008; Vilajosana *et al.*, 2008; Dammeier *et al.*, 2011). Signals were band-pass filtered between 2 and 20 Hz. We used the following relationship to estimate the seismic energy E_s (Vilajosana *et al.*, 2008):

$$E_s = 2\pi rphc \int_{t_0}^{t_1} u_{env}(t)^2 e^{\alpha r}\, dt \qquad (1)$$

where t_0 and t_1 are the manually picked onset and end times of the seismic signal, *r* is the distance between the event and the recording station (2040 m for the North Pillar and 1400 m for the South Pillar), *p* is the ground density (assumed at 2700 kg m^{-3}), *h* is the thickness of the layer through which surface waves propagate (taken as one wavelength of Rayleigh waves, h=200 m for a frequency centroid of 10 Hz), *c* is the phase velocity of Rayleigh waves (assumed at 2000 m s^{-1}), u_{env}(t) is the envelope of the ground velocity obtained using the Hilbert transform. The damping factor α accounts for an elastic attenuation of seismic waves and is calculated using the maximum amplitudes of the rockfall seismic signal at two seismic stations and the distances between source and sensor. Since only one seismic station is available for the study site, the value (of α =8.8 x10^{-4} m^{-1}) estimated for Mount Saint-Eynard rockfalls was used, with a frequency centroid of 10 Hz (Le Roy *et al.*, 2019).

Rockfall seismic signals can also be characterized by their equivalent magnitude, using the same relations as for earthquakes. Local magnitude can be estimated from the seismic energy using the Gutenberg-Richter magnitude-energy relation (Kanamori and Anderson, 1975).

$$Log\ E_s = 1.5M_L + 4.8 \qquad (2)$$

We then calibrated a relation between the magnitude M_L of a rockfall event and its volume *V*. We assumed a relation in the form of (Le Roy *et al.*, 2019):

$$M_L = a\ log_{10}(V) - b \qquad (3)$$

For each time interval between two TLS or UAV surveys, we selected all events within this time interval. We then optimized the parameters *a* and *b* of equation (3) in order to minimize the root-mean-square error between the logarithm of volume estimated from TLS or UAV surveys and the cumulated volume estimated from the signal magnitude using equation (3). We found *a=0.84* and *b=1.38*, in good agreement with the results obtained by Le Roy *et al.* (2019) for rockfalls in the Chartreuse massif (French Alps).

3. Results

3.1. Precursory observations and geomorphological development of the rock face

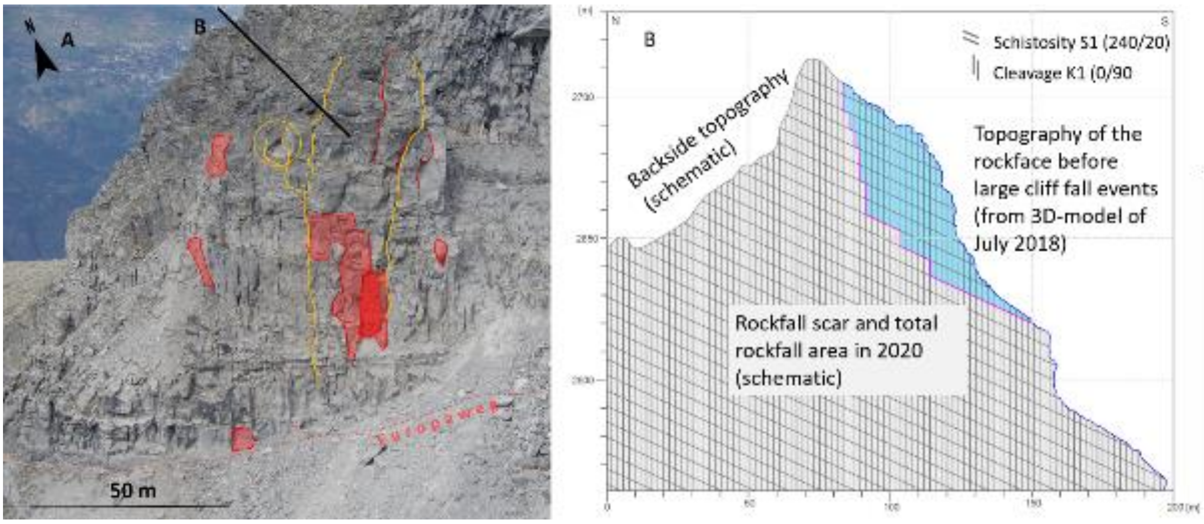

Figure 5. Close up of Grosse Grabe North Pillar: a) Before any large rockfall occurred (photograph of 06/09/2018). Precursory indicators of destabilization could already be observed by terrestrial laser scanner (red) and automatic camera (yellow) in forms of small scale rockfall (< 10^3 m^3) and fracture opening. And b) geological cross section showing main schistosity and cleavage related to the total rockfall area and scar surface (derived from ShapeMetric3D software).

Two isolated boulder falls (10^1-10^2 m^3) were detected visually for the first time in January and May 2017 (Figure 3b, Figure 5 a, yellow circle), launching a more accurate survey of Grosse Grabe North Pillar and the adjacent rock wall by Terrestrial laser scans (TLS) in July 2017. In the following winter seasons of 2018 and 2019, small magnitude rockfall (< 10^3 m^3) were observed, occurring in between January and May (Figure 5 a, red polygons). In the summer of 2019 and 2020 larger magnitude rockfalls (10^4 m^3) and cliff falls (10^4-10^6 m^3) followed up each other in close succession, with no single rockfall event in the associated winter period (November 2019 – April 2020).

Besides rockfall, deformation of the Grosse Grabe North Pillar was also observed as an outward displacement with more pronounced displacement in the upper part, indicating a tilting or toppling motion. Cleft opening and widening, associated with this outward displacement, could be observed on two different time scales. TLS data indicated that cleft opening at the upper part of the rock pillar was already ongoing in 2017 and 2018, gradually opening up (Figure 5 a, red lines), while automatic camera imagery revealed an accelerated cleft widening four to five weeks before the first cliff fall in August 2019 (Figure 5 a, yellow lines, Figure S2, suppl. material). The observed displacement and associated cleft opening is therefore considered to be the main precursory factor for the sudden large rock- and cliff fall events having occurred in the summer of 2019 and 2020. The observed displacement also has a clear seasonal pattern with an average monthly displacement by a factor of 1.2 to 2 times bigger in summer (June-September) than in winter (October-May) (Figure 6). Three different zones can be distinguished (Figure 6, 7, 8): (i) zone 1 that collapsed in the summer of 2019 (Figure 7 c, Figure 8 b), and corresponds to the Grosse Grabe North Pillar, displayed on Figure 5, (ii) zone 2 that collapsed almost entirely in the summer of 2020 (Figure 7 d, Figure 8 c,d) and (iii) zone 3 that has not yet experienced any large rockfall up to the summer of 2021 (Figure 7 d, Figure 8 d). However, rockfall is still to be expected in this zone, where a cumulative displacement of up to 47 cm has been (Figure 6, 7 d).

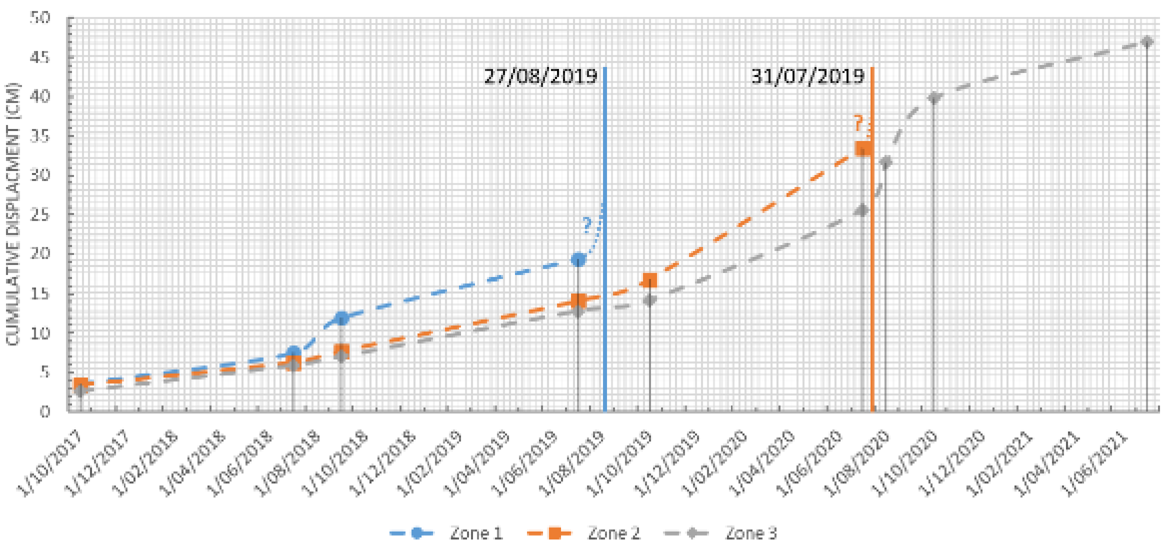

Figure 6.: Cumulative displacement based on the third quartile (75th percentile) of all the measured displacement for Grosse Grabe North Pillar (Zone 1) and the adjacent rock face (zone 2 and zone 3). Collapse date is indicated for zone 1 and 2, while zone 3 has not experienced any significant rockfall up to the summer of 2021. Dotted line is an interpolation of the measurements.

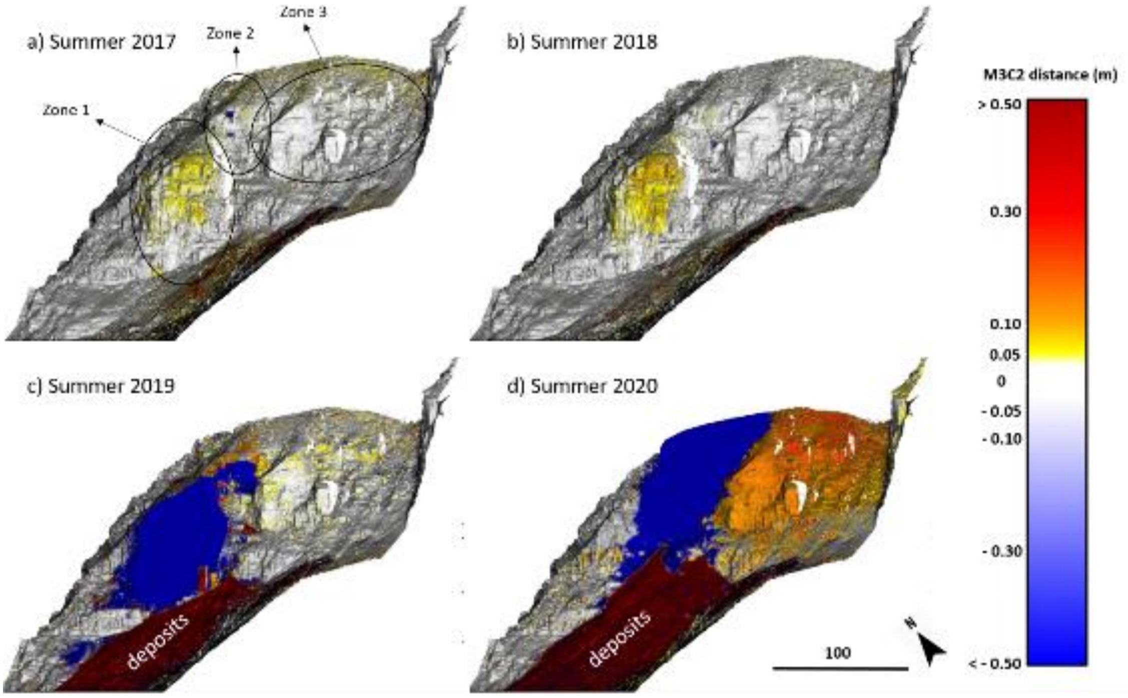

Figure 7.: The forward displacement of the Grosse Grabe North Pillar (zone 1) and adjacent rock wall (zone 2 and 3) in the summer of a) 2017, b) 2018, c) 2019 and d) 2020. Observed changes are relative to the scan at the beginning of summer and are statistically significant at the 95% confidence level with a minimum level of detection of 3 cm. Background is a hillshade based on terrestrial laser scan surveys.

A wet rockfall scar was observed by the automatic camera for several days after large cliff falls, in otherwise dry conditions, suggesting the presence of ice and thus potentially thawing permafrost. This was observed for the first time at the end of August 2019, when a total scar depth of 22.5 m (Figure 5 b), measured by the TLS data, was reached from the preluding rock- and cliff fall events (Figure 9 a). In the summer of 2020, the presence of compact ice could be confirmed with more detailed UAV imagery (Figure 9 b, c) after fresh rock- and cliff fall events occurring on 29 July and 31 July 2020 respectively. The latter was a very large cliff failure, with a calculated volume of 21 392 ± 6418 m^3 based on the UAV imagery (Video S1; Suppl. Material). Following rockfall events (Table 2) diminished the width of the upper ridge even further by removing 17.1 m of rock. This resulted in a very narrow and highly fractured ridge of a width of only 8 m, as calculated by using the UAV imagery (Figure 8 c). Finally, the ridge collapsed after several large rock- and cliff fall events that took place on 14 August 2020 between 8h30 and 11h, accounting for the largest volume of 33 880 ± 10164 m^3 recorded so far (Table 2, Figure 8 d). A laser scan performed on the 19 August 2020 measured a total volume of 94 523 ± 3781 m^3 for the entire summer period (01 July – 19 August 2020), this being an underestimation because no surface comparison could be made where the ridge was denudated (estimated to have had a volume of ± 3000 m^3 based on the seismic signal and thus within the error margin of the TLS derived volume).

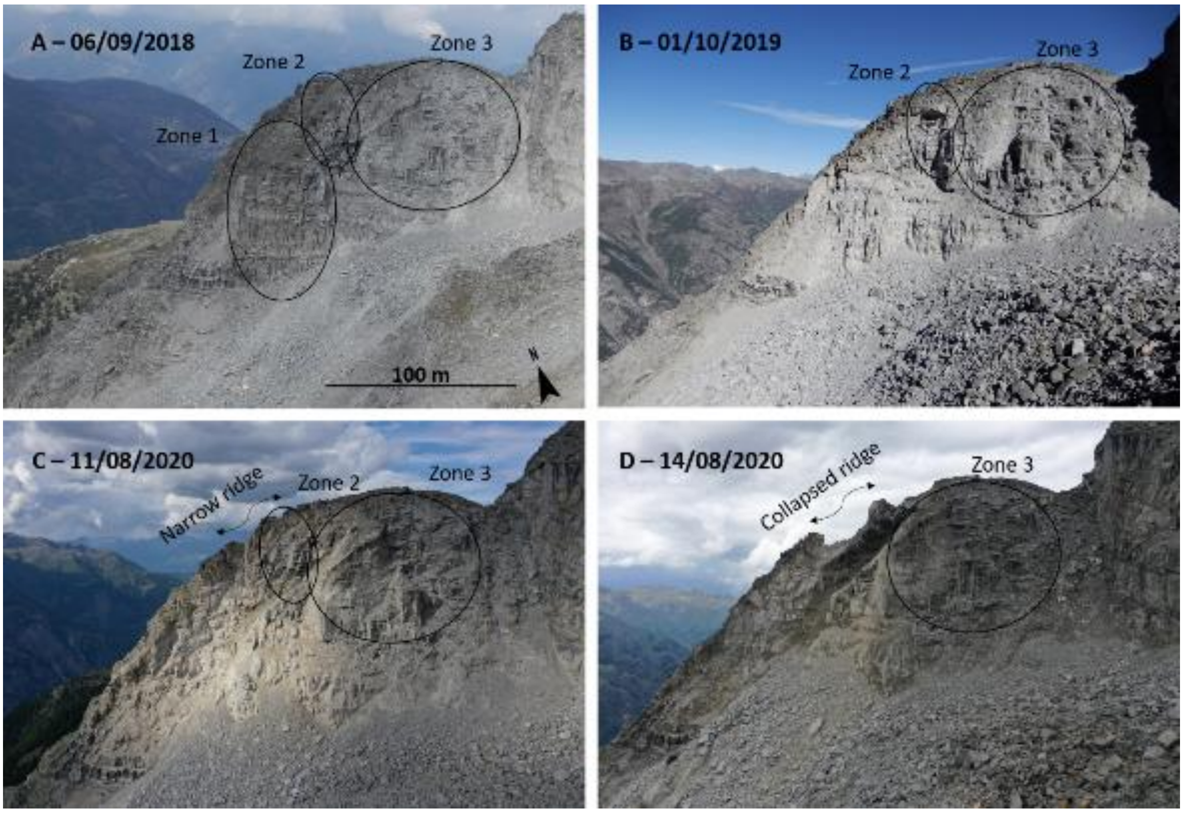

Figure 8: Geomorphological development of Grosse Grabe North Pillar and the adjacent rock wall: a) Situation before the large rock- and cliff fall events of the summer of 2019 and b) after the summer of 2019 and the situation c) before and d) after the largest cliff fall event on 14 August 2020, causing the collapse of part of the ridge. All imagery taken under a (sub-)horizontal angle.

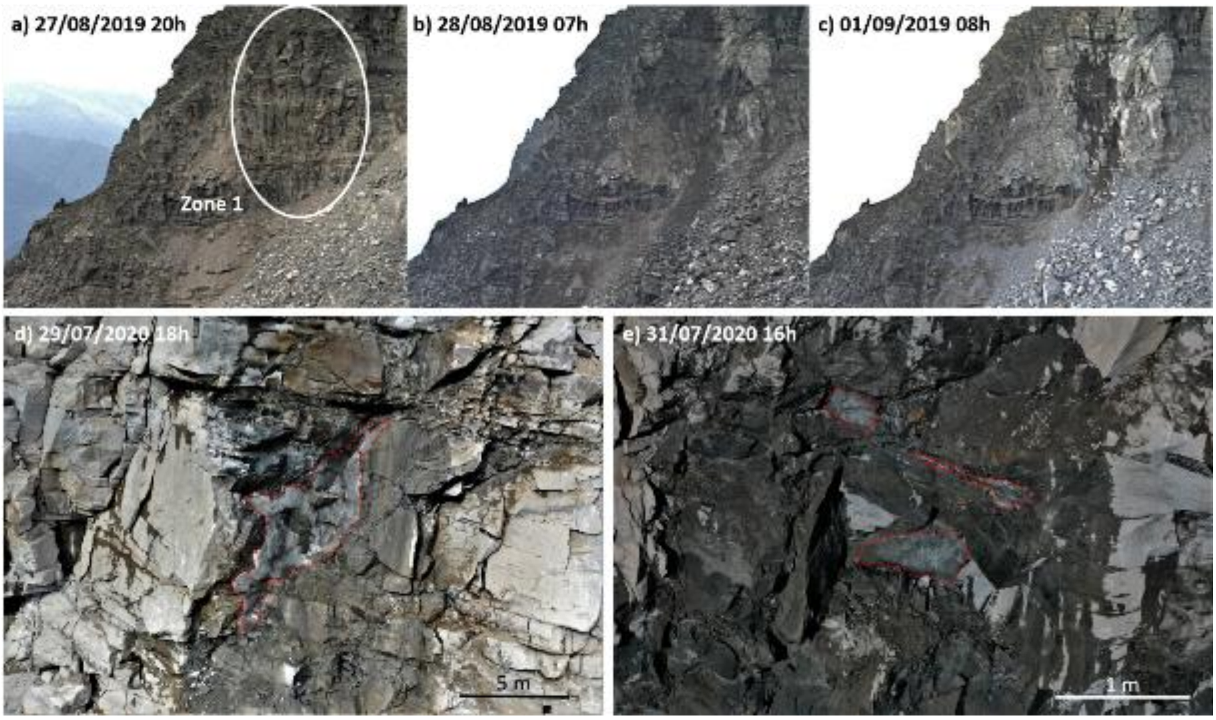

Figure 9.: Exposed ice at Grosse Grabe North Pillar (Zone 1), indicating the possible presence of permafrost, which occurs deep in the rock face following a cliff fall event, a) automatic camera imagery of 2019 showing an image before and b) after the cliff fall event of 27 August 2019, and c) the wet rockfall scar a couple of days after in otherwise dry conditions, d) UAV imagery shortly after the event of 29 July 2020 showing compacted ice and e) UAV imagery after the event of 31 July 2020 showing smaller ice patches, indicated by a red dotted line. All imagery taken under a (sub-)horizontal angle.

3.2. The timing and extent of rockfall events

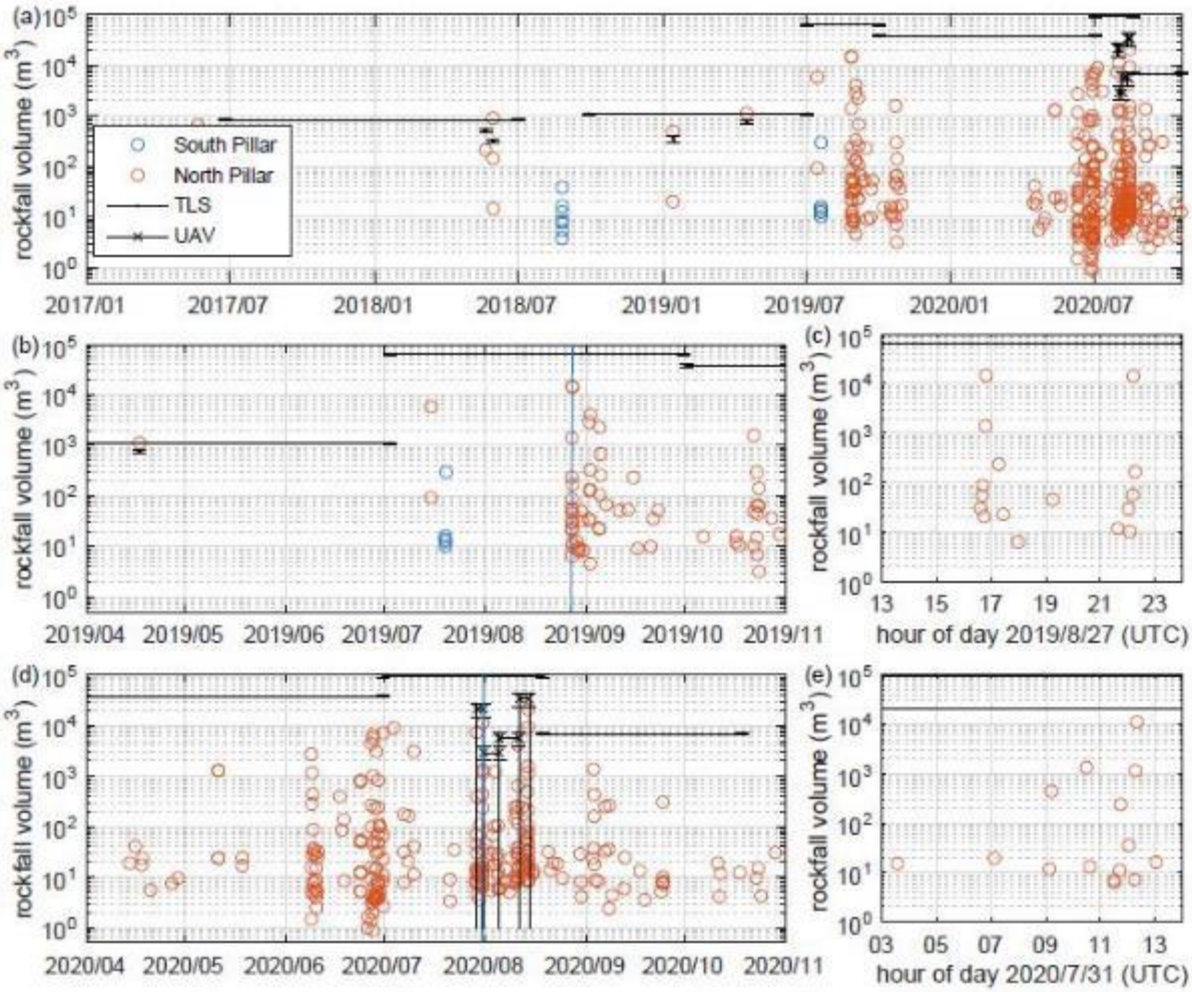

Figure 10.: Timeline of rockfall events (a) for the full time period between January 2017 and September 2020, (b) for the period April 2019 – November 2019, with c) highlighting the first large cliff fall events on 27/08/2019, d) for the period April 2020 – November 2020, with e) highlighting the cliff fall event on 31/07/2020, showing precursory rockfall. Red (North Pillar) and Blue (South Pillar) circles represent individual rockfall volumes estimated from the seismic signals using equations (1-3). Black dots and black crosses represent respectively cumulated volumes in each time interval between TLS or UAV surveys.

Table 2.: The topographic data gathered and the resulting rockfall volumes calculated

Date (dd/mm/jjjj)	Topographic data derived from:	Number of scans or photographs	Number of points in point cloud	Rockfall volumes since previous survey (m^3)	Cumulated volume from seismic signals (m^3) (95% confidence interval)
26/06/2017	TLS	1	15 500 167		
06/10/2017	TLS	1	16 313 071	0	0
03/07/2018	TLS	1	20 191 249	831 ± 33	1265 (416-3845)
29/09/2018	TLS	1	18 350 987	0	92 (30-281)

03/07/2019	TLS	1	13 628 608	1 102 ± 44	1635 (538-4969)
01/10/2019	TLS	1	20 566 426	63 138 ± 2526	49 192 (16181-149548)
01/07/2020	TLS	2	32 640 662	37 697 ± 1508	42 466 (13969-129102)
19/08/2020	TLS	2	24 300 449	94 523 ± 3781	76 991 (25325-234061)
19/10/2020	TLS	2	38 576 084	6846 ± 274	3208 (1055-9752)
29/07/2020	UAV	139	21 045 119		
31/07/2020	UAV	79	21 208 056	21 392 ± 6418	59 779 (19663-181734)
05/08/2020	UAV	116	16 630 783	2 880 ± 864	6025 (1982-18317)
11/08/2020	UAV	139	18 593 781	5 559 ± 1668	6025 (1982-18317)
14/08/2020	UAV	149	14 383 741	33 880 ± 10164	34 260 (11269-104155)
		Total measured volume (26/06/2017-19/10/2020)		204 137 ± 8166	175700 (57794-534147)

TLS: terrestrial laser scanning, UAV: uncrewed aerial vehicle

Analysing the seismic data resulted in a high temporal record of all the rock- and cliff fall events that occurred at Grosse Grabe North pillar and adjacent rock wall. The few events that occurred at Grosse Grabe South Pillar, out of reach for the automatic camera and the TLS/UAV data could also be quantified. In total, the seismic logger detected 339 rockfall events for the North Pillar and 12 for the South Pillar in the timespan of four years (2017-2020) (Figure 10) (Table S1, Suppl. Material). Most of the timely isolated and significant events at the North Pillar could be confirmed by the automatic camera, indicating the zone of failure (Figure S2, Suppl. Material). Isolated and small scale rockfall events occurred before the summer of 2019, in mid-winter (January) and in springtime (April - May). This changed in the summer of 2019, with the first isolated larger rockfall event occurring in mid-July (10^3 - 10^4 m^3) preluding larger cliff fall events (10^4 m^3) around the end of August (Figure 10 b, c). Rockfall continued to occur throughout September and October, but decreasing in magnitude (Figure 10 b). No rockfall occurred during the winter of 2019-2020 (November – May). Rockfall events started again in April-May 2020 (Figure 10 d). By the end of June and throughout July and August several cliff fall events (10^4 m^3) were observed again (Figure 10 d, e). The last event of around 500 m^3 occurred in late October. No significant rockfall events were observed in the following winter (2020-2021). It can be deduced from the seismic dataset (Figure 10) that 82% of the larger rock- and cliff fall events (> 5000 m^3, N=11) are preluded by two or more smaller events. In all cases, precursory rockfall happened within the hour before a large failure, often only a few minutes before. Only half of the larger rockfall events experienced precursory rockfall several hours before (Figure 10 e). Post-failure small-scale boulder falls (≤ 10^2 m^3) happened some minutes up to a few hours after the collapse are common as well (Figure 10 c). After that, rockfall activity ceased for several days up to weeks before rockfall events became numerous again (≤ 10^3 m^3). At the same time, these events announced the detachment of the next larger volumes of rockfall. This process continued until late summer, when finally rockfall activity ceased until spring.

The cross correlation between the meteorological data (temperature and precipitation) and rockfall activity suggests that rockfall occurs more frequently a few days after precipitation or a warming event, but the correlation is very weak (peak correlation of around 0.1 for daily precipitation for a time delay of 2 days) and barely significant. This could be because of the short time dataset (2017 – 2020), where the events are grouped together in burst of activities. However, it is clear that rockfall activity mostly develops in the summer only (Figure 10). Half of the large rock- and cliff fall events we observed happened in the second half of the summer (end of July, August), when temperatures are in general warmer and when summer air temperature had the time to warm the rock temperature at depth. Moreover, most large rock- and cliff fall (8 out of 11) occurred in the (late) afternoon. In addition, the three rockfall events that occurred in June 2020 were preluded by weekly higher temperatures (7.9 ± 0.3 °C) than are the average for June (5.7 ± 2.7 °C) based on data of the PermaSense weather station (2013-2020). This is also the case with the four large rockfall events between 29 July – 14 August 2020, preluded by significantly higher temperatures (10.5 ± 1.2 °C) than normal for that time of the year (7.8 ± 1.5 °C).

3.3. Rockwall erosion rates and the deposited material

A total rockfall volume of 204 137 ± 8166 m^3 was measured based on high resolution TLS and UAV derived topographic data (Table 2, 2017-2020). Since no significant rockfall was observed by the automatic camera since 2011, we assume this to be the total rockfall volume across a full 10-year period of direct observations. This corresponds to a mean rockwall erosion rate of 214 ± 8.9 mm a^{-1} for Grosse Grabe North Pillar and the adjacent rockwall (Figure 1 c, TLS extent). If we include the indirect observations of rockfall occurrence based on historical aerial photographs (Figure 2), we can assume that the measured rockfall volume (2017-2020) was the only significant rockfall across a 30-year period. This would correspond to a mean rockwall erosion rate of 71.2 ± 2.8 mm a^{-1} .

More than 200 000 m^3 of material was deposited below the Grosse Grabe North Pillar in between 2017 and 2020, based on the measured and estimated rockfall volumes. These deposits overlay most of the intermediate rupture zone between the upper intact part and the terminal tongue of the Grosse Grabe rock glacier (Figure 2). The measured deposited volumes within the range of the TLS scan (Figure 11) are 99 625 ± 3985 m^3 for 2019-2020. If we assume an initial porosity of 30%, in line with the porosity of blocky talus (Sass and Wollny, 2001) and that of other rockfall deposits in an alpine setting (Sanders *et al.*, 2013), we get an estimated deposited volume of 70 000 m^3 . As settling of the deposit sets in, a downward movement of up to two meters could be observed in late summer – autumn 2020 at the apex of the rock fall deposit cone. The motion is restricted to the deposited area and is diminishing further down, indicating crushing and a decrease in porosity as main process for the movement caused (Figure 11). Single large boulders were also transported into the Grosse Grabe torrent, outside the range of the scan (Video S1; Suppl. material). This occurred at least 11 times according to the imagery of the automatic camera, corresponding with the largest rock- and cliff fall events (> 5000 m^3) during the summer of 2019 and 2020. Rock debris is considered ending up in the torrent each time it is discernibly overpassing the rock glacier front.

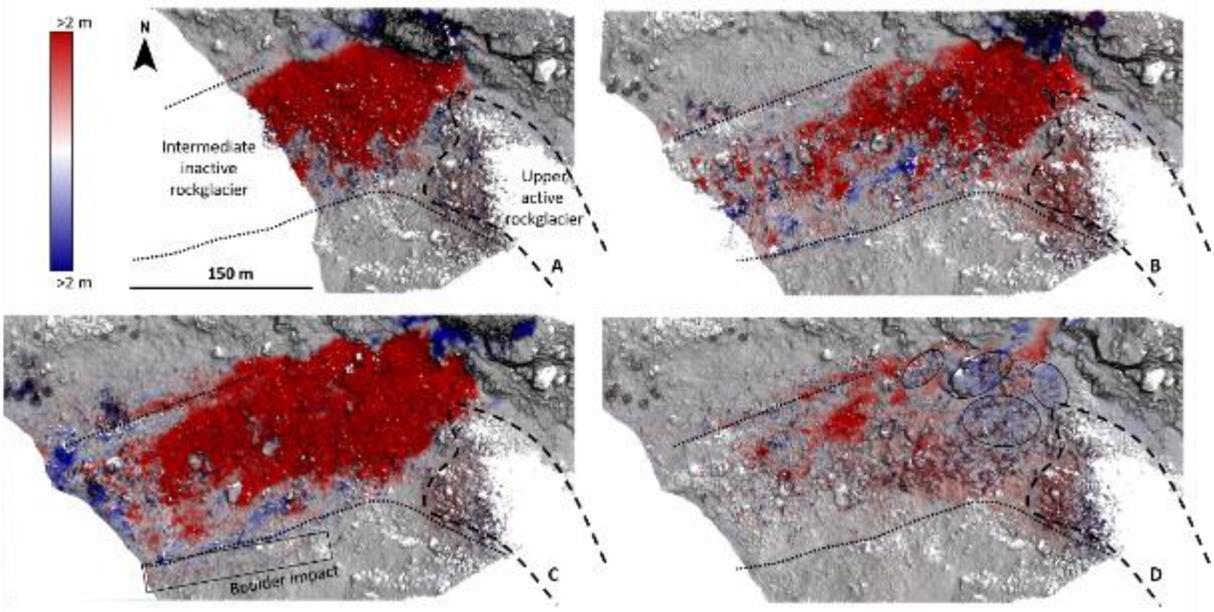

Figure 11.: Rockfall deposits (thickness perpendicular to slope) on the talus slope below the rock face for a) the summer of 2019, b) the winter of 2019-2020, c) the first part of the summer of 2020 (1 July – 19 August) and d) the second part of the summer of 2020 (19 August – 19 October), the latter showing compression of the deposits under their own weight in the upper part of the debris cone (indicated by the ellipses). Zones with no data is due to differences in the scan extent.

4. Discussion

4.1. Limitations of the methods

Uncertainties remain present within the collected high resolution datasets, even though different methods were integrated and the record starts two years prior to the main destabilisation period. The TLS data serves well to detect and quantify precursory deformation before the large rockfall events in the summer of 2019 and 2020 but was limited to a Level Of Detection (LoD) of 3 cm and the monitoring interval. Precursory deformation in zone 2 and 3 was close to this LoD at the onset of the monitoring period (Figure 6). (Near-) continuous and more detailed quantification of rockwall deformation and cleft opening can alternatively be achieved by ground-based InSAR (Gischig *et al.*, 2009) and the in-situ installation of crackmeters (Weber *et al.*, 2017). However, such methods are expensive and depend highly on site accessibility respectively. Imagery from the time-lapse camera was also able to detect the outward movement, already occurring before 2017 (Figure S1, Suppl. Material), but could only be quantified after the launch of the TLS survey. From the additional scan performed in August 2020, we know that the largest displacement occurs at the end of the summer season (19/08-19/10/2020). The measured winter (October – May) displacement likely occurs mostly in autumn, although this cannot be confirmed due to the restrictions of the monitoring interval. The monitoring interval does not allow rockfall volumes to be calculated either if they were released from the same zone. The largest rockfall events also caused topographic occlusion due to the single scan position, leading to an underestimation of the rockfall volume. This is somewhat corrected by the five UAV surveys launched before and after the largest events in the summer of 2020, not suffering from occlusion. However, the occluded volumes, calculated by subtracting the UAV derived volumes with the TLS derived volumes, fall completely within the error margins of the TLS data (< 4 – 5 %) and would thus not affect the results significantly. Besides the visual confirmation of ice in the rockfall scars only hours after the events, this shorter monitoring interval also allows the optimising of the established relationship between measured volumes and the seismic signal (Figure 12). Overall, we achieve a good fit between the estimated volume based on the seismic data and the ones more directly measured by TLS and UAV point cloud meshes (Table 2). The seismic data collection is the only monitoring method in this study that allows all rockfall events to be recorded. This way, pre- and post-event rockfall events could be analysed. The seismic data of only one sensor could be used for the rockfall period. This has the disadvantage that rockfall locations cannot be estimated precisely. It is therefore crucial to have the time-lapse imagery to validate the observed seismic signals. Only one event with a large amplitude was recorded by the seismic sensor and could not be detected on the time-lapse imagery. Likely, this rockfall event with an estimated volume of 300 m^3 occurred elsewhere in the area.

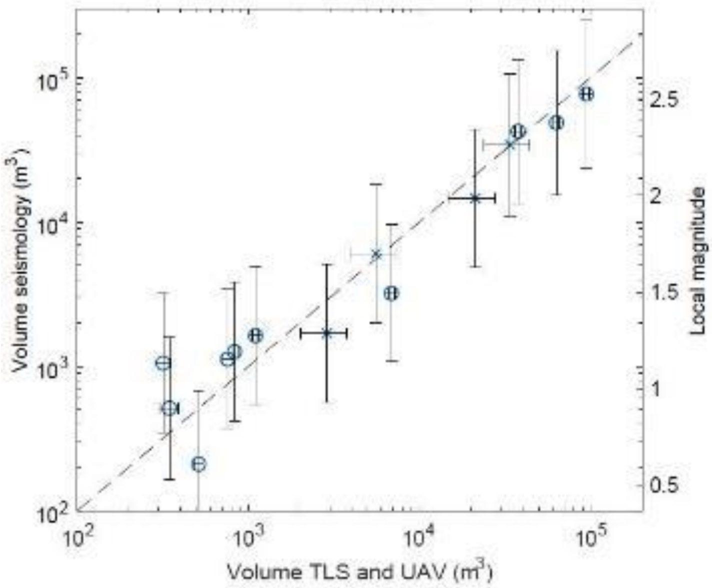

Figure 12. Volume estimated from the seismic signals and equivalent local magnitude as a function of rockfall volume estimated from TLS (circles) or UAV surveys (crosses) (summing over all events in each time interval). Error bars are 95% confidence intervals given by a linear fit of logarithms of volumes.

4.2. Structural predisposition, potential preparatory factors and observed precursory indicators to rock slope destabilisation

At Grosse Grabe North Pillar, the gentle dipping angle of 20° and cleavage-parallel weak layers susceptible to disruption in combination with deep, persistent and sub-vertical fracture systems favour large rockfalls (Figure 5 b). Already in 1982 and the following years, similar consecutive events took place (Figure 2). Probably the same structural conditions were at play. This could be a geological legacy of the glacial retreat after the Last Glacial Maximum, known to have affected and cause rock fractures in the Matter Valley (Leith *et al.*, 2014). The structural predisposition of the studied rock face entails several potential failure mechanisms, acting on fracture level, to operate as preparatory factors. Irreversible movements of fractures can be caused by thermal fluctuations (Gunzburger, Merrien-Soukatchoff and Guglielmi, 2005; Collins and Stock, 2016; Bakun-Mazor *et al.*, 2020), water pressure (Hasler, Gruber and Beutel, 2012; Walter *et al.*, 2019), freezing and thawing of water in the rock mass (Hasler, Gruber and Beutel, 2012; Weber *et al.*, 2017) and seismic vibrations (Luckman, 2013; Bakun-Mazor *et al.*, 2020) and a combination of all of these processes.

The cumulative and repetitive nature of thermally induced failure mechanisms are considered an important preparatory factor for rockfall in fractured rock masses exposed to high temperature oscillations (Gunzburger, Merrien-Soukatchoff and Guglielmi, 2005; Collins and Stock, 2016; Draebing, Krautblatter and Hoffmann, 2017; Bakun-Mazor *et al.*, 2020). Although no in situ rock temperatures were measured at the south facing rock face of Grosse Grabe, similar south-exposed rockwalls yield a daily temperature variation of up to 16.5°C compared to only 4°C for north-facing rockwalls as a result of solar radiation differences (Draebing and Mayer, 2021). While daily temperature changes only penetrate down to shallow depths (up to 0.4 m) (Gunzburger, Merrien-Soukatchoff and Guglielmi, 2005), seasonal thermal changes can propagate deeper in highly fractured bedrock (up to 100 m) due to air convection (Gischig *et al.*, 2011). Thus, Grosse Grabe North pillar is likely to be very susceptible to this thermally induced failure mechanism due to large daily and seasonal temperature variations, the presence of a gently inclined sliding plane and the high fracture density of the rock (Figure 5 b). Moreover, such thermally induced displacements are typically observed when temperatures are rising during summer (Bakun-Mazor *et al.*, 2020). This matches well with the observed seasonality of the pre-failure displacement observed at Grosse Grabe, with a displacement that was more pronounced by a factor of 1.2 to 2 in summer (Figure 6, 7). The observed larger irreversible displacements in summer might also indicate the potential role of water-related processes, such as changes in water pressure (Walter *et al.*, 2019) and advective warming by water percolation (Hasler *et al.*, 2011; Weber *et al.*, 2017), for example due to snow or permafrost meltwater (Weber *et al.*, 2017) and summer rainfall (Walter *et al.*, 2019). However, we found no indication for the latter in the meteorological data, possibly due to the long offset-time until rockfall occurrence. In addition, the catchment area of the rock face is small and mostly free of snow. Moreover, water pressure might not be dominant in strongly fractured and steep rock because of its high drainage ability (Phillips *et al.*, 2016; Weber *et al.*, 2017). Seismic vibrations due to earthquakes might influence fracture stability and prepare and trigger rockfall (Luckman, 2013). 2634 earthquake events were measured by the seismic sensor since 2015 and this might have played a role in rock wall destabilisation. However, the earthquakes observed for our analysed period never exceeded a ground motion of 2 mm s^{-1}, too weak to trigger any rockfall as compared to a ground motion 0.5 m s^{-1} suggested as a minimum threshold for triggering landslides or rockfalls (Keefer, 1984).

Temperature cycles also drive cryogenic processes in the studied rock wall, due the confirmed presence of ice (Figure 9). Although observed winter rockfall activity is limited, frost weathering can still act as a preparatory factor for rockfall occurrence by subcritical cracking and progressively reducing rock strength (Draebing and Krautblatter, 2019). Frost weathering might be highly effective at Grosse Grabe North Pillar, as indicated by modelling results of rock walls at similar elevation and exposition (Draebing and Mayer, 2021), preparing rockfall that is than subsequently triggered by processes in summer, such as thermal stresses described above. Fracture displacement due to cryogenic processes is often linked to ice pressure and thus widening of the fractures at the onset of freezing (Draebing, Krautblatter and Hoffmann, 2017; Weber *et al.*, 2017). However, we observed a decrease in the displacement in winter, which we link to the cementing effect of permanent and seasonal ice as a consequence of a rapid cooling of the clefts due to colder air temperatures and probably to air circulation in the fractured rock (Gruber and Haeberli, 2007; Hasler, Gruber and Beutel, 2012). This cementing effect of the ice-bonded discontinuities decreases progressively during the summer due to a decrease in stiffness and strength of the ice at warmer temperatures (Davies, Hamza and Harris, 2001). This hypothesis is supported by the presence of ice in the deeper bedrock (at least at 15 m depth), affecting the sub-vertical fractures. Permafrost degradation might therefore be a potential preparatory factor, considering the long-term warming of the area.

Both precursory rockfall and deformation are known to sometimes prelude rock- and cliff fall (Abellán *et al.*, 2010). From the moment fractures are subjected to large irreversible movements, driven by one or several of the mechanisms explained above, a critical state will slowly be reached (Hasler, Gruber and Beutel, 2012). A change in deformation geometry is detected approx. 1.5 years before the first significant collapse in zone 1 and zone 2. After this, large, irreversible movements are clearly observed at Grosse Grabe North Pillar, with an increase in pre-failure displacement by a factor of 2-3.5 prior to the collapse (Figure 6). This increase in outward displacement is mainly observed in the upper part of Grosse Grabe North Pillar, with the rock volume staying the same, indicating a tilting or toppling type of failure developed (Abellán *et al.*, 2010). This type of failure is often linked to sub-vertical fractures (Goodman and Kieffer, 2000). At Grosse Grabe, the failure of sub-vertical fractures in the lower rockwall are believed to be the cause of the toppling motion. The isolated rockfall events before 27 August 2019 are considered to be precursory rockfalls preluding the destabilisation phase in the summer of 2019 and 2020.

4.3. Potential triggers leading to progressive rockwall collapse

Most rockfall occurred in the warmer half of the year and no large rockfall occurred in winter. In addition, large follow-up rockfall events (> 5000 m^3) occurred when weekly temperatures were warmer than average for that time of the year and occurred mostly in the (late) afternoon. Next to thermal stresses, this could also indicate that the melting of ice-filled joints (or decreasing of their resistance to stress) (Davies, Hamza and Harris, 2001) close to the surface plays a role. The depth at which temperature change is perceptible in bedrock after a week of unusually high temperature is likely to be no more than 1 m based on borehole data (PERMOS, 2016). Moreover, larger events within this destabilisation phase were also announced by small-scale rockfall within hours of the larger volume, similar to small magnitude rockfall events during hot summers (Figure 10 e). These rockfall events are typically associated to permafrost presence at shallow depths, triggered by active layer thickening (Ravanel, Magnin and Deline, 2017). Such type of rockfall had not been observed at Grosse Grabe before the rockfall event of 27 august 2019 (Figure 10 c), indicating that permafrost was not present at the sub-surface of the south-facing rock, confirming model results

(Boeckli *et al.*, 2012; Magnin *et al.*, 2017). However, permafrost presence was confirmed when rockfall exposed massive ice (Figure 9), which often occurs after failures in permafrost-affected rock (Gruber and Haeberli, 2007; Mamot *et al.*, 2018; Kenner, Bühler, *et al.*, 2019; Walter *et al.*, 2019). According to numerical models of subsurface temperature fields in ridge topography (Noetzli *et al.*, 2007), this likely corresponds to the base of the permafrost developed at the north face, at the distance of 50 – 70 m. We exclude the possibility that this is seasonal ice, considering it is exposed at the time when we at least expect seasonal ice to persist (at the end of summer). Since the large cliff fall on 27 August 2019 (Figure 10 c) permafrost has been exposed and prone to rapid degradation due to thermal adjustment and subsequent active layer thaw. This thermal adjustment, together with the redistribution of stress from preceding large rockfalls (Nishii and Matsuoka, 2012; Stock *et al.*, 2012), leads to progressive failure of the rock face and the observed rapid sequence of events (Figure 10). The bounding ice quickly melted, not only at the surface but also at shallow depths in the clefts, quickly changing the strength of the rock mass and favouring the detachment of the next volume. This process did not occur in winter and ceased in September 2019, when cold weather conditions kept the exposed face frozen and thus dry. Large rockfall events are to be expected for the next years at Grosse Grabe North pillar, because of the dense fracturation of the rock face and the observed pre-failure displacement of up to 47 cm in zone 3 (Figure 6, 7). However, no change in geometry (i.e. cleft widening) has been observed in this zone. The displacement is characterised by a homogenous movement of the face along the dipping plane, suggesting a deep-seated gravitational deformation or sackung taking place.

4.4. Observed rock wall erosion rates and their implication for future development

High magnitude rockfall events, such as observed in this study, are highly relevant for shaping alpine landscapes (McColl and Draebing, 2019). Logically, observations of rock wall retreat made in a period of high rockfall activity tend to overestimate long-term rock wall erosion rates. Erosion rates based on a short term record should therefore be interpreted with care (Hartmeyer *et al.*, 2020). Commonly, long-term rock wall retreat rates for alpine periglacial environments are around 1 mm a^{-1} (Ballantyne, 2018; Matsuoka, 2019). Higher rates are reported in deglaciating cirques, with a rate of 1.9 mm a^{-1} to 10.3 mm a^{-1} on short time scales (4-6 yrs) (Kenner *et al.*, 2011; Hartmeyer *et al.*, 2020). Even the most conservative rock wall retreat rate (71.2 ± 2.8 mm a^{-1}) calculated for Grosse Grabe (assuming the rockfall events of 2017-2020 are the only major activity since 1990 for the entire extent of the monitored rock face (Figure 1)) is still very high compared to rock wall erosion rates of other studies. Hartmeyer et al. (2020) reported very high retreat rates (57.32 ± 0.67 mm a^{-1}) for recently deglaciated areas along highly fractured weakness zones close to the glacial surface. Although the monitored rock face in this study is not recently deglaciated, highly fractured lithology does play an important role in the observed high rock wall retreat rates. In addition, and as discussed in the previous section, we believe that the exposure of the base of the permafrost from the North side of the ridge triggered progressive failure of the rock wall and is responsible for the unusually high erosion rates. Although interpretation should be done with care, our results suggest that permafrost degradation in these specific settings has the potential to alter the rock wall retreat rate drastically on a short time scale. In the future, air temperatures are expected to increase in the European Alps (Gobiet *et al.*, 2014). Because of this, and the change in associated cryogenic and thermal stresses acting on rock walls, Draebing, Krautblatter, and Hoffmann (2017) expect a shift from cryogenic driven rockfall on north-exposed rock walls to thermally driven rockfall on south-facing rockwalls. If this occurs in narrow ridge topography in areas experiencing marginal permafrost, exposure of deep bedrock permafrost developed from the north side could lead to progressive failure of the rock wall, as observed in this study. Although rock wall erosion rates are expected to decrease at the elevation of our study site due to a shift of frost weathering to higher elevations (Draebing and Mayer 2021), they might first increase due to scenario's similar to the one presented in this study. Moreover, the observed temporal clustering of the rockfall events has an important implication for hazard management, potentially endangering hikers making use of the hiking track in summer.

5. Conclusion

This research presents a detailed temporal and spatial record of the processes and events before, during and after consecutive large rock- and cliff falls that occurred at a rock face at Grosse Grabe in Mattertal (Western Swiss Alps) in 2019 and 2020. This rockfall record proved to be highly valuable to gain insight in the preconditioning, preparatory and triggering factors involved, of use for understanding similar rockfall happening elsewhere in the European Alps. We also show the potential of combining multiple close-range remote sensing data for the detection of rockfall in high mountain environments, where challenging field conditions do not allow in-situ measurements. The integration of both high resolution topography datasets derived from TLS and UAV with seismic observations resulted in a detailed overview of the exact timing and estimated volumes of all individual rockfall events, as validated by the automatic camera.

The initial cause of the large consecutive rock- and cliff falls (10^3 - 10^6 m^3) that occurred in the summers of 2019 and 2020 are considered to be of geological nature with a pre-existing mesh of discontinuities (mostly tectonic clefts and schistosity bedding). The south exposure makes this densely fractured rock wall vulnerable for thermally induced failure mechanism on different timescales, highlighted by the increased irreversible displacement observed in summer, the occurrence of rockfall mostly in the second half of summer and in the (late) afternoon. The observed outward displacement of the rock face prior to any rockfall suggest a toppling failure mechanism related to sub-vertical fractures in the rock wall. A change in deformation geometry was observed 1.5 years before any significant collapse, with an increase in the outward displacement at the top of the rock face. The deformation was probably affecting frozen rock as well, indicating that permafrost degradation is a potential preparatory factor. A large rockfall event at the end of August in 2019 exposed deep bedrock permafrost, believed to be the base of the permafrost developed from the north side of the ridge, triggering progressive failure of the rock wall due to thermal adjustment. This process quickly melted the exposed and the subsurface ice and together with the unloading caused large rock- and cliff fall events to occur in a short succession in the summer of 2019 and 2020. These events were often preluded by precursory small-scale rockfall, believed to be triggered by active layer thickening, hours before the larger volume detached. All rockfall activity ceased in the winter season when the process of thermal adjustment is stalled due to colder temperatures. All site specific conditions, such as the dense fracturation, the southerly aspect, the gentle dipping of the schistosity bedding and the large cliff falls exposing deep bedrock permafrost, lead locally to very high rock wall erosion rates.

DATA AVAILABILITY STATEMENT

The datasets used and/or analysed during the current study are available from the corresponding author on reasonable request.

CONFLICT OF INTEREST

The authors declare that there is no conflict of interest.

References

Abellán, A. *et al.* (2010) 'Detection and spatial prediction of rockfalls by means of terrestrial laser scanner monitoring', *Geomorphology*. Elsevier, 119(3–4), pp. 162–171. doi: 10.1016/j.geomorph.2010.03.016.

Allen, S. and Huggel, C. (2013) 'Extremely warm temperatures as a potential cause of recent high mountain rockfall', *Global and Planetary Change*, 107, pp. 59–69. doi: 10.1016/j.gloplacha.2013.04.007.

Baer, P. *et al.* (2017) 'Changing debris flow activity after sudden sediment input: a case study from the Swiss Alps', *Geology Today*, 33(6), pp. 216–223. doi: 10.1111/gto.12211.

Bajni, G., Camera, C. and Apuani, T. (2020) 'Bajni, Greta, Corrado Camera, and Tiziana Apuani. "Deciphering Rainfall and Freeze thaw cycles as long-term preparatory factors for alpine rockfalls', in *EGU General Assembly Conference Abstracts.*, p. 6793.

Bakun-Mazor, D. *et al.* (2020) 'Thermally-Induced Wedging–Ratcheting Failure Mechanism in Rock Slopes', *Rock Mechanics and Rock Engineering*, 53(6), pp. 2521–2538. doi: 10.1007/s00603-020-02075-6.

Ballantyne, C. K. (2018) *Periglacial Geomorphology*. John Wiley & Sons.

Bearth, P. (1978) 'Geologischer Atlas der Schweiz 1:25 000, Karte 71. Blatt 1308. Swisstopo: St. Niklaus'.

Beniston, M. *et al.* (2018) 'The European mountain cryosphere: A review of its current state, trends, and future challenges', *Cryosphere*, 12(2), pp. 759–794. doi: 10.5194/tc-12-759-2018.

Boeckli, L. *et al.* (2012) 'Permafrost distribution in the European Alps: Calculation and evaluation of an index map and summary statistics', *Cryosphere*, 6(4), pp. 807–820. doi: 10.5194/tc-6-807-2012.

Collins, B. D. and Stock, G. M. (2016) 'Rockfall triggering by cyclic thermal stressing of exfoliation fractures', *Nature Geoscience*. Nature Publishing Group, 9(5), pp. 395–400. doi: 10.1038/ngeo2686.

Cook, K. L. and Dietze, M. (2019) 'Short Communication: A simple workflow for robust low-cost UAV-derived change detection without ground control points', *Earth Surface Dynamics Discussions*, 7(4), pp. 1–15. doi: 10.5194/esurf-2019-27.

D'Amato, J. *et al.* (2016) 'Influence of meteorological factors on rockfall occurrence in a middle mountain limestone cliff', *Natural Hazards and Earth System Sciences*, 16(3), pp. 719–735. doi: 10.5194/nhess-16-719-2016.

Dammeier, F. *et al.* (2011) 'Characterization of alpine rockslides using statistical analysis of seismic signals', *Journal of Geophysical Research: Earth Surface*. Blackwell Publishing Ltd, 116(4). doi: 10.1029/2011JF002037.

Davies, M. C. R., Hamza, O. and Harris, C. (2001) 'The effect of rise in mean annual temperature on the stability of rock slopes containing ice-filled discontinuities', *Permafrost and Periglacial Processes*. John Wiley & Sons, Ltd., 12(1), pp. 137–144. doi: 10.1002/ppp.378.

Delaloye, R. *et al.* (2013) 'Rapidly moving rock glaciers in Mattertal', *Jahrestagung der Schweizerischen Geomorphologischen Gesellschaft*, (i), pp. 21–31.

Delaloye, R. *et al.* (2014) *Blockgletscher und Hangrutschungen in Permafrostgebieten Departement für Geowissenschaften*, *Blockgletscher und Hangrutschungen in Permafrostgebieten, Projekt 'Mattertal' (2009-2013), Gemeinde St.-Niklaus und Randa, Abschlussbericht 2013. non publié, 121p.*

Delaloye, R. and Morard, S. (2011) 'Le glacier rocheux déstabilisé du Petit-Vélan (Val d'Entremont, Valais): morphologie de surface, vitesses de déplacement et structure interne', in *La géomorphologie alpine: entre patimoine et contrainte. Actes du colloque de la Société Suisse de Géomorphologie, 3-5 septembre 2009, Olivone (Géovisions n° 36). Institut de géographie, Université de Lausanne.*, pp. 197–210.

Deparis, J. *et al.* (2008) 'Analysis of rock-fall and rock-fall avalanche seismograms in the French Alps', *Bulletin of the Seismological Society of America*. GeoScienceWorld, pp. 1781–1796. doi:

10.1785/0120070082.

Dietze, M., Mohadjer, S., *et al.* (2017) 'Seismic monitoring of small alpine rockfalls-validity, precision and limitations', *Earth Surface Dynamics*, 5(4), pp. 653–668. doi: 10.5194/esurf-5-653-2017.

Dietze, M., Turowski, J. M., *et al.* (2017) 'Spatiotemporal patterns, triggers and anatomies of seismically detected rockfalls', *Earth Surface Dynamics*, 5(4), pp. 757–779. doi: 10.5194/esurf-5-757-2017.

Draebing, D. and Krautblatter, M. (2019) 'The Efficacy of Frost Weathering Processes in Alpine Rockwalls', *Geophysical Research Letters*, 46(12), pp. 6516–6524. doi: 10.1029/2019GL081981.

Draebing, D., Krautblatter, M. and Dikau, R. (2014) 'Interaction of thermal and mechanical processes in steep permafrost rock walls: A conceptual approach', *Geomorphology*. Elsevier, 226, pp. 226–235. doi: 10.1016/j.geomorph.2014.08.009.

Draebing, D., Krautblatter, M. and Hoffmann, T. (2017) 'Thermo-cryogenic controls of fracture kinematics in permafrost rockwalls', *Geophysical Research Letters*, 44(8), pp. 3535–3544. doi: 10.1002/2016GL072050.

Draebing, D. and Mayer, T. (2021) 'Topographic and Geologic Controls on Frost Cracking in Alpine Rockwalls', *Journal of Geophysical Research: Earth Surface*. Blackwell Publishing Ltd, 126(6). doi: 10.1029/2021JF006163.

Dussauge, C., Grasso, J.-R. and Helmstetter, A. (2003) 'Statistical analysis of rockfall volume distributions: Implications for rockfall dynamics', *Journal of Geophysical Research: Solid Earth*. American Geophysical Union (AGU), 108(B6). doi: 10.1029/2001jb000650.

Eissler, H. K. and Kanamori, H. (1987) 'A single-force model for the 1975 Kalapana, Hawaii, Earthquake', *Journal of Geophysical Research*. American Geophysical Union (AGU), 92(B6), p. 4827. doi: 10.1029/jb092ib06p04827.

Fischer, L. *et al.* (2011) 'Monitoring topographic changes in a periglacial high-mountain face using high-resolution DTMs, Monte Rosa East Face, Italian Alps', *Permafrost and Periglacial Processes*. John Wiley & Sons, Ltd, 22(2), pp. 140–152. doi: 10.1002/ppp.717.

Fischer, L *et al.* (2012) 'On the influence of topographic, geological and cryospheric factors on rock avalanches and rockfalls in high-mountain areas', *Natural Hazards and Earth System Science*, 12(1), pp. 241–254. doi: 10.5194/nhess-12-241-2012.

Fischer, L. *et al.* (2012) 'On the influence of topographic, geological and cryospheric factors on rock avalanches and rockfalls in high-mountain areas', *Natural Hazards and Earth System Science*, 12(1), pp. 241–254. doi: 10.5194/nhess-12-241-2012.

Fischer, M. *et al.* (2016) 'Application and validation of long-range terrestrial laser scanning to monitor the mass balance of very small glaciers in the Swiss Alps', *Cryosphere*, 10(3), pp. 1279–1295. doi: 10.5194/tc-10-1279-2016.

Gardner, J. S. (1983) 'Rockfall frequency and distribution in the Highwood Pass area, Canadian Rocky

Mountains', *Zeitschrift für Geomorphologie*, 27(3), pp. 311–324. doi: 10.1127/zfg/27/1983/311.

Gischig, V. *et al.* (2009) 'Identification of active release planes using ground-based differential InSAR at the Randa rock slope instability, Switzerland', *Natural Hazards and Earth System Science*. Copernicus GmbH, 9(6), pp. 2027–2038. doi: 10.5194/nhess-9-2027-2009.

Gischig, V. S. *et al.* (2011) 'Thermomechanical forcing of deep rock slope deformation: 1. Conceptual study of a simplified slope', *Journal of Geophysical Research: Earth Surface*, 116(4), p. F04010. doi: 10.1029/2011JF002006.

Gobiet, A. *et al.* (2014) '21st century climate change in the European Alps-A review', *Science of the Total Environment*, 493, pp. 1138–1151. doi: 10.1016/j.scitotenv.2013.07.050.

Goodman, R. E. and Kieffer, D. S. (2000) 'Behavior of Rock in Slopes', *Journal of Geotechnical and Geoenvironmental Engineering*. American Society of Civil Engineers (ASCE), 126(8), pp. 675–684. doi: 10.1061/(asce)1090-0241(2000)126:8(675).

Gruber, S. (2004) 'Permafrost thaw and destabilization of Alpine rock walls in the hot summer of 2003', *Geophysical Research Letters*, 31(13), p. L13504. doi: 10.1029/2004GL020051.

Gruber, S. and Haeberli, W. (2007) 'Permafrost in steep bedrock slopes and its temperatures-related destabilization following climate change', *Journal of Geophysical Research: Earth Surface*, 112(2), pp. 1–10. doi: 10.1029/2006JF000547.

Guillemot, A. *et al.* (2020) 'Seismic monitoring in the Gugla rock glacier (Switzerland): ambient noise correlation, microseismicity and modelling', *Geophysical Journal International*. Oxford University Press (OUP), 221(3), pp. 1719–1735. doi: 10.1093/gji/ggaa097.

Gunzburger, Y., Merrien-Soukatchoff, V. and Guglielmi, Y. (2005) 'Influence of daily surface temperature fluctuations on rock slope stability: Case study of the Rochers de Valabres slope (France)', *International Journal of Rock Mechanics and Mining Sciences*. Pergamon, 42(3), pp. 331–349. doi: 10.1016/j.ijrmms.2004.11.003.

Haeberli, W. and Beniston, M. (1998) 'Climate change and its impacts on glaciers and permafrost in the Alps', *Ambio*, 27, pp. 258–265.

Hartmeyer, I. *et al.* (2020) 'A 6-year lidar survey reveals enhanced rockwall retreat and modified rockfall magnitudes/frequencies in deglaciating cirques', *Earth Surface Dynamics*. Copernicus GmbH, 8(3), pp. 753–768. doi: 10.5194/esurf-8-753-2020.

Hasler, A. *et al.* (2011) 'Advective heat transport in frozen rock clefts: Conceptual model, laboratory experiments and numerical simulation', *Permafrost and Periglacial Processes*. John Wiley & Sons, Ltd, 22(4), pp. 378–389. doi: 10.1002/ppp.737.

Hasler, A., Gruber, S. and Beutel, J. (2012) 'Kinematics of steep bedrock permafrost', *Journal of Geophysical Research: Earth Surface*. John Wiley & Sons, Ltd, 117(1), p. n/a-n/a. doi: 10.1029/2011JF001981.

Hasler, A., Gruber, S. and Haeberli, W. (2011) ‘Temperature variability and offset in steep alpine rock and ice faces’, *Cryosphere*, 5(4), pp. 977–988. doi: 10.5194/tc-5-977-2011.

Helmstetter, A. and Garambois, S. (2010) ‘Seismic monitoring of Schilienne rockslide (French Alps): Analysis of seismic signals and their correlation with rainfalls’, *Journal of Geophysical Research: Earth Surface*, 115(3), pp. 1–15. doi: 10.1029/2009JF001532.

Hendrickx, H. *et al.* (2020) ‘Talus slope geomorphology investigated at multiple time scales from high-resolution topographic surveys and historical aerial photographs (Sanetsch Pass, Switzerland)’, *Earth Surface Processes and Landforms*, p. esp.4989. doi: 10.1002/esp.4989.

Huggel, C. *et al.* (2012) ‘Ice thawing, mountains falling-are alpine rock slope failures increasing’, *Geology Today*. John Wiley & Sons, Ltd, 28(3), pp. 98–104. doi: 10.1111/j.1365-2451.2012.00836.x.

Kanamori, H. and Anderson, D. L. (1975) ‘Theoretical basis of some empirical relations in seismology’, *Bulletin of the Seismological Society of America*, 65(5), pp. 1073–1095.

Kanamori, H. and Given, J. W. (1982) ‘Analysis of long-period seismic waves excited by the May 18, 1980, eruption of Mount St Helens - a terrestrial monopole?’, *Journal of Geophysical Research*. John Wiley & Sons, Ltd, 87(B7), pp. 5422–5432. doi: 10.1029/JB087iB07p05422.

Keefer, K. D. (1984) ‘Landslides caused by earthquakes’, *GSA Bulletin*, 95(4), pp. 406–421. doi: https://doi.org/10.1130/0016-7606(1984)95<406:LCBE>2.0.CO;2.

Kenner, R. *et al.* (2011) ‘Investigation of rock and ice loss in a recently deglaciated mountain rock wall using terrestrial laser scanning: Gemsstock, Swiss Alps’, *Cold Regions Science and Technology*. Elsevier, 67(3), pp. 157–164. doi: 10.1016/j.coldregions.2011.04.006.

Kenner, R., Noetzli, J., *et al.* (2019) ‘Distinguishing ice-rich and ice-poor permafrost to map ground temperatures and ground ice occurrence in the Swiss Alps’, *Cryosphere*, 13(7), pp. 1925–1941. doi: 10.5194/tc-13-1925-2019.

Kenner, R., Bühler, Y., *et al.* (2019) *Ereignisanalyse. Felssturz und Lwine vom 19.3.2019 am Flüela Wisshorn (Davos, Graubünden)*.

Krautblatter, M. and Dikau, R. (2007) ‘Towards a uniform concept for the comparison and extrapolation of rockwall retreat and rockfall supply’, *Geografiska Annaler, Series A: Physical Geography*. Blackwell Publishing Ltd, 89(1), pp. 21–40. doi: 10.1111/j.1468-0459.2007.00305.x.

Krautblatter, M., Funk, D. and Günzel, F. K. (2013) ‘Why permafrost rocks become unstable: A rock-ice-mechanical model in time and space’, *Earth Surface Processes and Landforms*, 38(8), pp. 876–887. doi: 10.1002/esp.3374.

Krautblatter, M. and Moore, J. R. (2014) ‘Rock slope instability and erosion: Toward improved process understanding’, *Earth Surface Processes and Landforms*. John Wiley & Sons, Ltd, pp. 1273–1278. doi: 10.1002/esp.3578.

Kummert, M. and Delaloye, R. (2018) ‘Mapping and quantifying sediment transfer between the front of rapidly moving rock glaciers and torrential gullies’, *Geomorphology*. Elsevier, 309, pp. 60–76. doi: 10.1016/j.geomorph.2018.02.021.

Kummert, M., Delaloye, R. and Braillard, L. (2018) ‘Erosion and sediment transfer processes at the front of rapidly moving rock glaciers: Systematic observations with automatic cameras in the western Swiss Alps’, *Permafrost and Periglacial Processes*, 29(1), pp. 21–33. doi: 10.1002/ppp.1960.

Lague, D., Brodu, N. and Leroux, J. (2013) ‘Accurate 3D comparison of complex topography with terrestrial laser scanner: Application to the Rangitikei canyon (N-Z)’, *ISPRS Journal of Photogrammetry and Remote Sensing*. International Society for Photogrammetry and Remote Sensing, Inc. (ISPRS), 82, pp. 10–26. doi: 10.1016/j.isprsjprs.2013.04.009.

Leinauer, J., Jacobs, B. and Krautblatter, M. (2020) ‘Process dynamics , real time monitoring and early warning at an imminent cliff fall (Hochvogel , Allgäu Alps)’, in *EGU General Assembly 2020*. Online, pp. EGU2020-19073.

Leith, K. *et al.* (2014) ‘Subglacial extensional fracture development and implications for Alpine Valley evolution’, *Journal of Geophysical Research: Earth Surface*. John Wiley & Sons, Ltd, 119(1), pp. 62–81. doi: 10.1002/2012JF002691.

Luckman, B. H. (2013) ‘Processes , Transport , Deposition , and Landforms : Rockfall’, in Shroder, J. F. (ed.) *Treatise on Geomorphology*. 7th edn. San Diego: Academic Press, pp. 174–182. doi: 10.1016/B978-0-12-374739-6.00162-7.

Magnin, F. *et al.* (2017) ‘Modelling rock wall permafrost degradation in the Mont Blanc massif from the LIA to the end of the 21st century’, *Cryosphere*. Copernicus GmbH, 11(4), pp. 1813–1834. doi: 10.5194/tc-11-1813-2017.

Mamot, P. *et al.* (2018) ‘A temperature-and stress-controlled failure criterion for ice-filled permafrost rock joints’, *Cryosphere*. Copernicus GmbH, 12(10), pp. 3333–3353. doi: 10.5194/tc-12-3333-2018.

Matsuoka, N. (2008) ‘Frost weathering and rockwall erosion in the southeastern Swiss Alps: Long-term (1994–2006) observations’, *Geomorphology*. Elsevier, 99(1–4), pp. 353–368. doi: 10.1016/j.geomorph.2007.11.013.

Matsuoka, N. (2019) ‘A multi-method monitoring of timing, magnitude and origin of rockfall activity in the Japanese Alps’, *Geomorphology*. Elsevier, 336, pp. 65–76. doi: 10.1016/j.geomorph.2019.03.023.

McColl, S. T. and Draebing, D. (2019) ‘Rock Slope Instability in the Proglacial Zone: State of the Art’, in. Springer, Cham, pp. 119–141. doi: 10.1007/978-3-319-94184-4_8.

Moore, J. R. *et al.* (2011) ‘Air circulation in deep fractures and the temperature field of an alpine rock slope’, *Earth Surface Processes and Landforms*. John Wiley & Sons, Ltd, 36(15), pp. 1985–1996. doi: 10.1002/esp.2217.

Nishii, R. and Matsuoka, N. (2012) ‘Kinematics of an alpine retrogressive rockslide in the Japanese Alps’, *Earth Surface Processes and Landforms*. John Wiley & Sons, Ltd, 37(15), pp. 1641–1650. doi:

10.1002/esp.3298.

Noetzli, J. *et al.* (2007) 'Three-dimensional distribution and evolution of permafrost temperatures in idealized high-mountain topography', *Journal of Geophysical Research: Earth Surface*, 112(2), p. F02S13. doi: 10.1029/2006JF000545.

PERMOS (2016) *Permafrost in Switzerland 2010/2011 to 2013/2014.* Edited by J. Noetzli, R. Luethi, and B. Staub. Glaciological Report (Permafrost) No. 12-15 of the Cryospheric Commission of the Swiss Academy of Sciences.

Phillips, M. *et al.* (2016) 'Seasonally intermittent water flow through deep fractures in an Alpine Rock Ridge: Gemsstock, Central Swiss Alps', *Cold Regions Science and Technology*. Elsevier, 125, pp. 117–127. doi: 10.1016/j.coldregions.2016.02.010.

Phillips, M. *et al.* (2017) 'Rock slope failure in a recently deglaciated permafrost rock wall at Piz Kesch (Eastern Swiss Alps), February 2014', *Earth Surface Processes and Landforms*. John Wiley and Sons Ltd, 42(3), pp. 426–438. doi: 10.1002/esp.3992.

Ravanel, L., Magnin, F. and Deline, P. (2017) 'Impacts of the 2003 and 2015 summer heatwaves on permafrost-affected rock-walls in the Mont Blanc massif', *Science of the Total Environment*. Elsevier B.V., 609, pp. 132–143. doi: 10.1016/j.scitotenv.2017.07.055.

Le Roy, G. *et al.* (2019) 'Seismic Analysis of the Detachment and Impact Phases of a Rockfall and Application for Estimating Rockfall Volume and Free-Fall Height', *Journal of Geophysical Research: Earth Surface*, 124(11), pp. 2602–2622. doi: 10.1029/2019JF004999.

Sala, Z., Hutchinson, D. J. and Harrap, R. (2019) 'Simulation of fragmental rockfalls detected using terrestrial laser scans from rock slopes in south-central British Columbia, Canada', *Natural Hazards and Earth System Sciences*, 19(11), pp. 2385–2404. doi: 10.5194/nhess-19-2385-2019.

Sanders, J. W. *et al.* (2013) 'The sediment budget of an Alpine cirque', *Bulletin of the Geological Society of America*. GeoScienceWorld, 125(1–2), pp. 229–248. doi: 10.1130/B30688.1.

Sass (2005a) 'Rock moisture measurements: Techniques, results, and implications for weathering', *Earth Surface Processes and Landforms*. John Wiley & Sons, Ltd, 30(3), pp. 359–374. doi: 10.1002/esp.1214.

Sass (2005b) 'Spatial patterns of rockfall intensity in the northern Alps', *Zeitschrift für Geomorphologie*, 138, pp. 51–65.

Sass (2005c) 'Temporal variability of rockfall in the Bavarian Alps, Germany', *Arctic, Antarctic, and Alpine Research*, 37(4), pp. 564–573. doi: 10.1657/1523-0430(2005)037[0564:TVORIT]2.0.CO;2.

Sass, O. and Wollny, K. (2001) 'Investigations regarding alpine talus slopes using ground-penetrating radar (GPR) in the Bavarian Alps, Germany', *Earth Surface Processes and Landforms*. John Wiley & Sons, Ltd, 26(10), pp. 1071–1086. doi: 10.1002/esp.254.

ShapeMetric3D (2021). Available at: https://3gsm.at/produkte/shape-metrix/ (Accessed: 19 October

2021).
Stock, G. M. *et al.* (2012) 'Progressive failure of sheeted rock slopes: the 2009–2010 Rhombus Wall rock falls in Yosemite Valley, California, USA', *Earth Surface Processes and Landforms*. John Wiley & Sons, Ltd, 37(5), pp. 546–561. doi: 10.1002/ESP.3192.

Stoffel, M. and Huggel, C. (2012) 'Effects of climate change on mass movements in mountain environments', *Progress in Physical Geography*. SAGE Publications, 36(3), pp. 421–439. doi: 10.1177/0309133312441010.

Stoffel, M., Tiranti, D. and Huggel, C. (2014) 'Climate change impacts on mass movements - Case studies from the European Alps', *Science of the Total Environment*, 493, pp. 1255–1266. doi: 10.1016/j.scitotenv.2014.02.102.

Study sites - Grosse Grabe (2021). Available at: https://www3.unifr.ch/geo/geomorphology/en/resources/study-sites/grosse-grabe.html (Accessed: 3 May 2021).

UZH - The PermaSense Consortium (2021). Available at: https://www.permasense.ch/en.html (Accessed: 28 September 2021).

Vilajosana, I. *et al.* (2008) 'Rockfall induced seismic signals: Case study in Montserrat, Catalonia', *Natural Hazards and Earth System Science*. European Geosciences Union, 8(4), pp. 805–812. doi: 10.5194/nhess-8-805-2008.

Walter, F. *et al.* (2019) 'Direct observations of a three million cubic meter rock-slope collapse with almost immediate initiation of ensuing debris flows', *Geomorphology*, p. 106933. doi: 10.1016/j.geomorph.2019.106933.

Weber, S. *et al.* (2017) 'Quantifying irreversible movement in steep, fractured bedrock permafrost on Matterhorn (CH)', *Cryosphere*, 11(1), pp. 567–583. doi: 10.5194/tc-11-567-2017.